Massive Star Clusters in Ongoing Galaxy Interactions: Clues to Cluster Formation

William C. Keel – University of Alabama
Kirk D. Borne – Institute for Science and Technology at Raytheon

Citation of published version:

Keel, W., Borne, K. (2003): Massive Star Clusters in Ongoing Galaxy Interactions: Clues to Cluster Formation. *The Astronomical Journal*, 126(3). DOI: 10.1086/377482

The Astronomical Journal, 126:1257–1275, 2003 September

MASSIVE STAR CLUSTERS IN ONGOING GALAXY INTERACTIONS: CLUES TO CLUSTER FORMATION[1]

William C. Keel[2]
Department of Physics and Astronomy, University of Alabama, Box 870324, Tuscaloosa, AL 35487

and

Kirk D. Borne
Institute for Science and Technology at Raytheon; and NASA Goddard Space Flight Center, Greenbelt, MD 20771
Received 2003 February 5; accepted 2003 June 12

ABSTRACT

We present *HST* WFPC2 observations, supplemented by ground-based Hα data, of the star-cluster populations in two pairs of interacting galaxies selected for being in very different kinds of encounters seen at different stages. Dynamical information and *n*-body simulations provide the details of encounter geometry, mass ratio, and timing. In NGC 5752/4 we are seeing a weak encounter, well past closest approach, after about 2.5×10^8 yr. The large spiral NGC 5754 has a normal population of disk clusters, while the fainter companion NGC 5752 exhibits a rich population of luminous clusters with a flatter luminosity function. The strong, ongoing encounter in NGC 6621/2, seen about 1.0×10^8 yr past closest approach between roughly equal-mass galaxies, has produced an extensive population of luminous clusters, particularly young and luminous in a small region between the two nuclei. This region is dynamically interesting, with such a strong perturbation in the velocity field that the rotation curve reverses sign. From these results, in comparison with other strongly interacting systems discussed in the literature, cluster formation requires a threshold level of perturbation, with stage of the interaction a less important factor. The location of the most active star formation in NGC 6621/2 draws attention to a possible role for the Toomre stability threshold in shaping star formation in interacting galaxies. The rich cluster populations in NGC 5752 and NGC 6621 show that direct contact between gas-rich galaxy disks is not a requirement to form luminous clusters and that they can be triggered by processes happening within a single galaxy disk (albeit triggered by external perturbations).

Key words: galaxies: individual (NGC 5752, NGC 5754, NGC 6621, NGC 6622) — galaxies: interactions — galaxies: star clusters

1. INTRODUCTION

Evidence connecting galaxy interactions to powerful star-forming events has accumulated from observations over a wide range of wavelengths, from the radio continuum to X-rays. This enhancement in star formation does not consist merely of exceptional numbers of normal H II regions. Among the most striking results from early *HST* observations of interacting and merging systems was the prevalence of luminous, presumably massive super–star clusters (SSCs). While a handful are sufficiently bright and isolated to have been picked out from earlier ground-based data (e.g., Schweizer 1982 and Lutz 1991), it was the improved resolution of *HST* (for an early example, using prerefurbishment data, see Whitmore et al. 1993) that revealed them as an important population. In particular, their high luminosity allows the possibility that these are in effect young globular clusters, if they have a "normal" initial-mass function continuing to low stellar masses. This would fit with the idea that strongly interacting and merging galaxies today can serve as a useful model for conditions early in galaxy formation, when more isolated galaxies (such as ours) formed similar clusters as well.

As reviewed by Whitmore (2000), much of the focus in relating SSCs to galaxy interactions has been in following the cluster populations during and after major mergers. These studies have shown a general correlation between the ages of the SSCs, as derived from modelling their broadband colors, and the age of the merger from dynamical considerations. Objects seen close to the time of merger—such as infrared-luminous galaxies—can have extensive populations of such clusters in their inner few kiloparsecs. The benchmark for young cluster populations has been the Antennae, NGC 4038/9 (Whitmore et al. 1999b). The remnant disks of both galaxies contain rich populations of clusters as bright as $M_V = -14$, with evidence for distinct star-forming events in various parts of the system. The luminosity function of these clusters is close to a power law with slope $\alpha = -2.1$, possibly more precisely described as a broken power-law form. The luminosity function of SSCs and its possible evolution are important in probing the connection between these young, massive clusters and old globular clusters.

Much of the interest in these cluster populations has centered on the question of whether they are massive enough to be genuine globular clusters and how this fits with the merging hypothesis for the formation of elliptical galaxies. This has driven many studies of the SSC population

[1] Based on observations with the NASA/ESA *Hubble Space Telescope*, obtained at the Space Telescope Science Institute, which is operated by the Association of Universities for Research in Astronomy, Inc., under NASA contract NAS 5-26555.

[2] Visiting Astronomer, WIYN Observatory, which is owned and operated by the WIYN Consortium, Inc., which consists of the University of Wisconsin, Indiana University, Yale University, and the National Optical Astronomy Observatory (NOAO), and at Kitt Peak National Observatory, NOAO. NOAO is operated by AURA, Inc., under cooperative agreement with the National Science Foundation.

to concentrate on merging systems of various dynamical properties (forming a rough age sequence) and on a few galaxies seen very strongly interacting. As reviewed by Whitmore (2000), there is a continuous color sequence that follows a plausible fading line from the young clusters in the Antennae to globular clusters in such ellipticals as M87. While this favors the idea that these are similar populations seen at various epochs, and thus that mergers form many elliptical galaxies and important parts of their globular cluster systems, the luminosity function of SSCs in many systems is well described as a power law, like that of ordinary open clusters in spiral galaxies and quite different from the approximately Gaussian distribution of the old, "genuine" globular clusters in both spirals and ellipticals. This makes the survival and evolution of the clusters over gigayear time spans crucial in telling whether there really is a continuous sequence all the way to old globular clusters.

In contrast to these considerations of the long-term evolution of these luminous clusters, rather few galaxies in "typical" interactions outside of merging conditions have been surveyed for SSCs to assess a link between immediate tidal events and star formation in such massive concentration. Such interacting pairs may offer a cleaner view of when and how clusters form, with the dynamical history more easily recovered than in advanced mergers and different regions still connected to different tidal histories. It would be especially helpful if we were to see very different star formation responses in two gas-rich galaxies in a pair, since the timing of encounter is identical. In an effort to specify what kinds of galaxy dynamics and timescales are involved in the formation of SSCs, we have observed the cluster populations in two interacting galaxy pairs in different extremes of the interaction process, both well before merging takes place. Using morphology and *n*-body simulations, we selected pairs in the early stages of a very strong tidal encounter (NGC 6621/2) and at a late stage in a weak encounter (NGC 5752/4, which is weak for the larger galaxy at least). One might expect some kind of threshold for formation of these massive clusters, since they are not numerous in undisturbed disks and may require such special processes as collisions of giant molecular clouds or assembly of massive clouds within a particular time. Larsen (2002) finds that only a fraction ($\sim$15%) of luminous "normal" spirals have any cluster as bright as $M_V = -12.0$ and that very rich cluster populations are needed to expect such examples for a typical power-law luminosity function. Given this evidence that the cluster populations in interacting systems result from unusual processes, the systems for which we can infer ages and levels of perturbation might then offer clues to where and when the clusters form.

2. OBSERVATIONS

2.1. *Selection and Properties of Galaxy Pairs*

We selected candidate pairs, starting with the samples observed by Keel et al. (1985) spectroscopically and in Hα imaging, to select systems with active star formation so we would be able to ask how much of this star formation occurs in SSCs. We sought pairs with morphologies suggesting a single encounter of only two galaxies, so that their histories could be inferred from comparison with the *n*-body atlas results from Howard et al. (1993), and lower redshifts for the highest sensitivity and linear resolution. From these criteria we settled on the pairs NGC 5752/4 and NGC 6621/2 to represent two extremes of the pair population. The pairs also offer additional contrasts in that NGC 5752 and NGC 5754 are of very different size and luminosity, and NGC 6621 is much more gas-rich than NGC 6622.

NGC 5752/4 is part of the apparent quartet Arp 297. Despite the interestingly close configuration of these galaxies, redshift information breaks this grouping into two separately interacting pairs differing in distance by a factor of 2 (Fig. 1). The figure also shows the outer tidal structure, which aids in reconstructing the dynamical history of the pair, including a faint tail running westward from NGC 5752. The redshift listed for NGC 5752 in NED is somewhat suspicious, being exactly the same as listed for NGC 5754. We have therefore reexamined the low-resolution spectrophotometric data from Keel et al. (1985, where it is listed as Arp 297C) from which we derive a heliocentric velocity 4325 ± 85 km s^{-1} from Hγ, Hβ, and [O III] emission. This agrees well with a newly available archived spectrum from the CfA *z*-machine,[3] which gives 4441 ± 24 km s^{-1} from absorption-line cross-correlation. Adopting a value of $H_0 = 70$ km s^{-1} Mpc^{-1} gives a linear scale of 316 pc arcsec^{-1} for this pair.

NGC 5754 exhibits a rich population of disk H II regions, and NGC 5752 shows multiple, very bright H II regions closely packed around its core (Kennicutt et al. 1987), satisfying our requirement for substantial star formation.

NGC 6621/2 (Arp 81, VV 247, CPG 534) is much more strongly disturbed, kinematically as well as morphologically (Reshetnikov & Silchenko 1990; Keel 1993, 1996). It is part of the original sequence of candidate merging pairs presented by Toomre (1977). The fainter galaxy in this case is an E/S0 system, whose redshift (like that of NGC 5752) is in some question from published data. Gas from the larger disk galaxy NGC 6621 is so widespread that emission lines putatively seen from NGC 6622 are almost certainly from the extended disk of NGC 6621, based both on the morphology and velocity continuity of the line emission. We therefore measured an absorption-line value to help in interpreting the history of this system (§ 4.1). We adopt a linear scale of 430 pc arcsec^{-1} for this pair, based on a mean redshift $cz = 6210$ km s^{-1}.

2.2. *HST Imaging*

Each galaxy pair was observed with WFPC2 in both *B* (F450W) and *I* (F814W) passbands. As it happened, both were observed within a single 24 hour span, on 1999 March 14 and 15. The filters were selected to provide a wide color baseline coupled with high efficiency and rejection of strong emission lines. The elongated pair NGC 6621/2 was placed in CCDs WF2 and WF3. For NGC 5752/4, the high surface brightness companion NGC 5752 was placed on the PC CCD, with NGC 5754 and its tidal arms spreading across all three WF CCDs. This placement turned out to be fortunate because of the crowding of the many luminous clusters found in NGC 5752. Total exposure time in each filter was 2600 s, each split into two individual exposures for cosmic-ray rejection. Mosaics of the WFPC2 images are shown in Figures 2 and 3. Data from the individual CCDs have been

[3] At http://tdc-www.harvard.edu/cgi-bin/arc/uzcsearch.

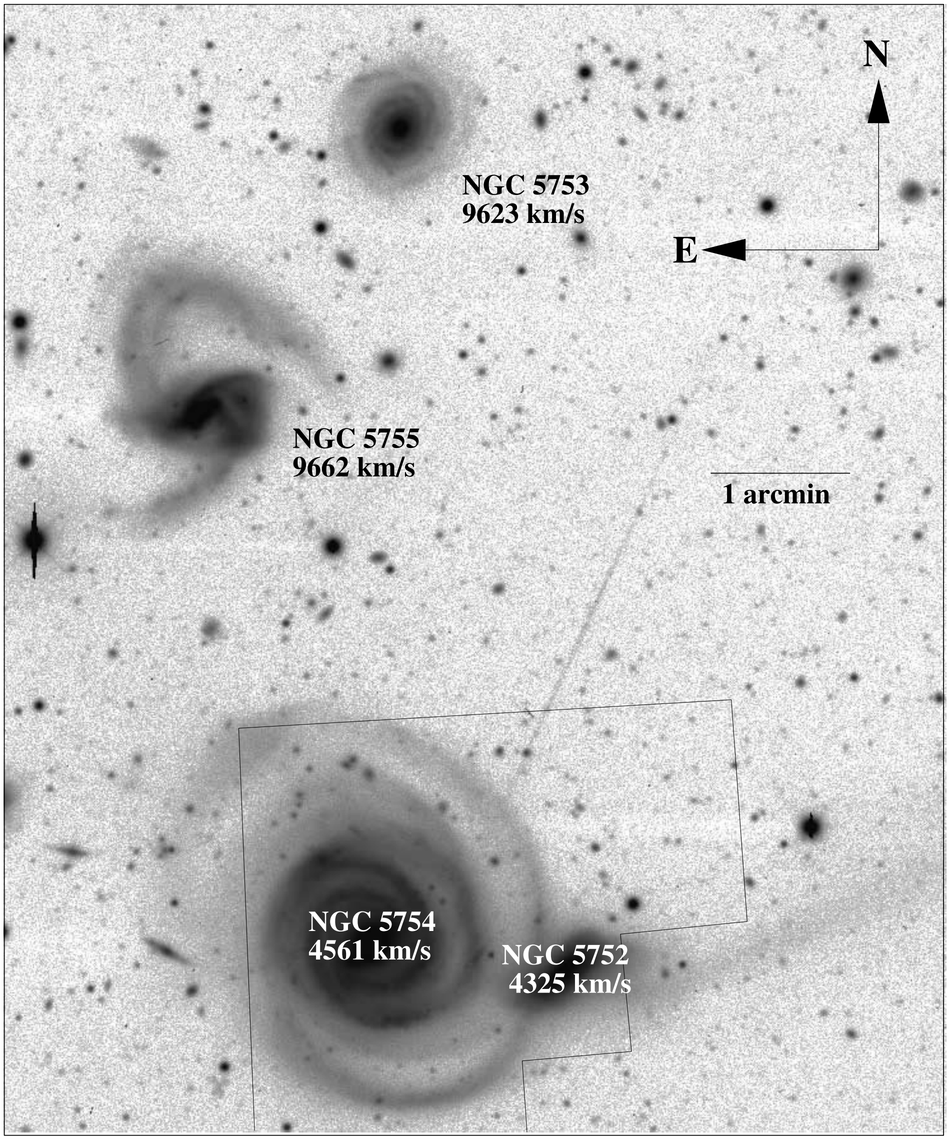

Fig. 1.—Two galaxy pairs of Arp 297, marked on a KPNO 4 m *R*-band image. Velocities are heliocentric. The WFPC2 observation footprint is indicated around NGC 5752/4. The image is shown with a pseudologarithmic intensity mapping to emphasize faint tidal structures. The field spans 5′.16 × 6′.19.

rebinned to a common astrometric frame for these figures, but cluster photometry was done on the original data.

We followed the photometric procedures of Whitmore et al. (1999b) as closely as the greater distance of our targets would allow, to be able to compare the cluster populations most directly with the well-observed Antennae system, NGC 4038/9. Cluster candidates were identified using the IRAF[4] implementation of DAOFIND and measured using aperture photometry (radius 0″.2 and curve-of-growth aperture correction of 0.70 mag) with a local background. For simplicity of analysis, we adopt a uniform flux threshold for candidate clusters across each galaxy, set by experiments with the number of false detections at a given detection threshold and removing a few spurious detections produced by the greater Poisson noise near the center of NGC 5754. As in similar studies, cluster colors are almost completely independent of aperture effects, with only 2%–7% changes in the fraction of encircled energy within the 0″.2 aperture expected across our wavelength baseline. We followed Holtzman et al. (1995) in assuming an aperture of radius 0″.5 to encompass 90% of the energy. Between 0″.2 and 0″.5 we find that the brightest clusters show a curve of growth similar to the point-source prediction (specifically, the brightest ones in NGC 5754 give a correction 0.23 mag, compared with a calculated value of 0.17 from the WFPC2 handbook). Residual photometric errors due to geometric distortion within the WFPC2 optics, which exist because the flat-field correction is set up to properly correct surface brightness rather than point-source intensity, should be less than 2% for the regions spanned by these galaxies. The role of foreground extinction should be quite modest for these pairs; the Schlegel, Finkbeiner, & Davis (1998) prescription gives $A_B = 0.20$, $A_I = 0.09$ for NGC 6621/2 at $b = 23°$, and $A_B = 0.05$, $A_I = 0.02$ for NGC 5752/4 at $b = +63°$. We fold these values into the respective photometric zero points. Charge-transfer effects are not very important even

[4] IRAF is distributed by NOAO, which is operated by AURA, Inc., under cooperative agreement with NSF.

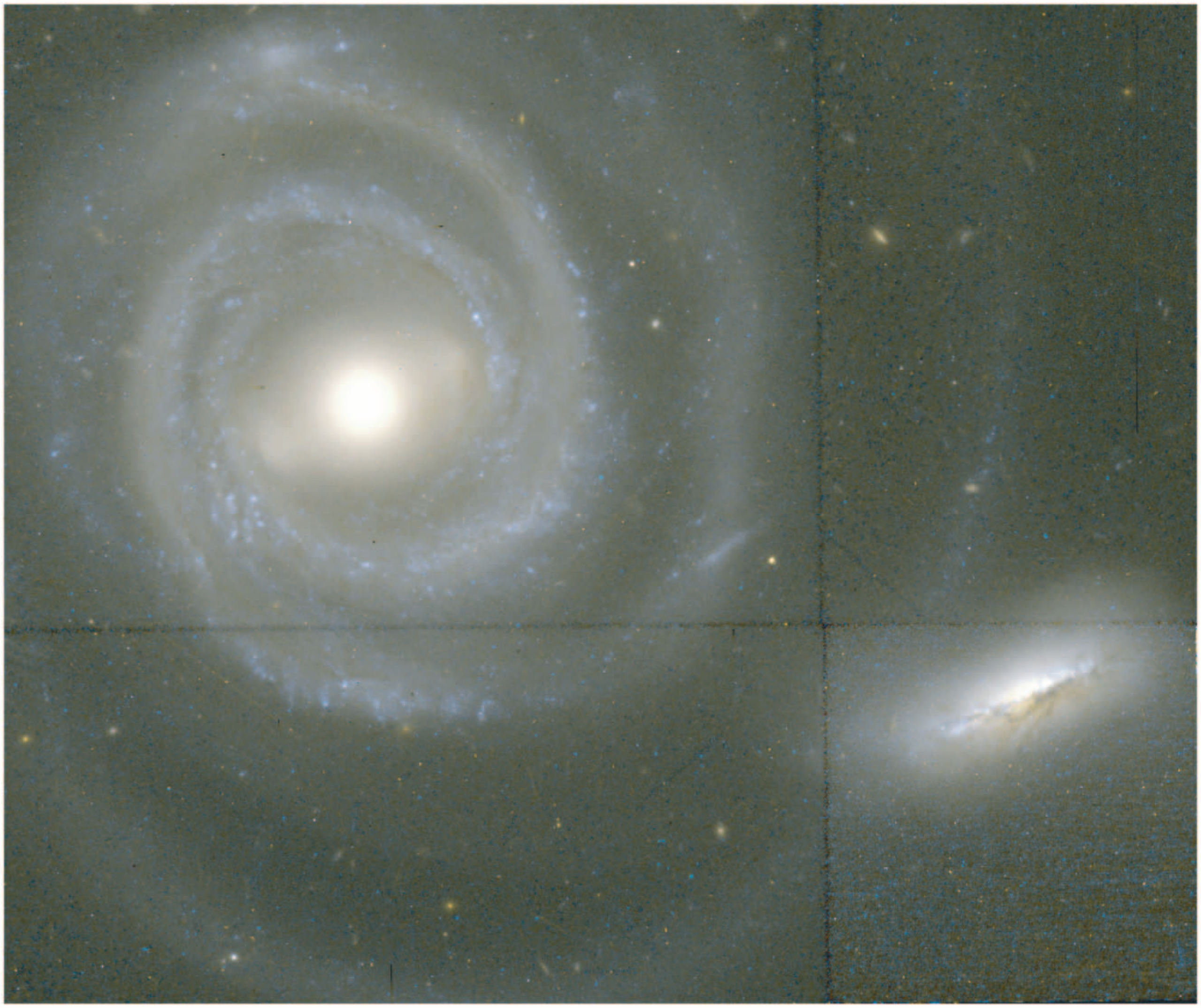

Fig. 2.—WFPC2 imagery of NGC 5752/4, shown as a color composite incorporating a synthetic green band taken as the mean of B and I, with a pseudologarithmic intensity scale. The regions shown covers $90'' \times 108''$; north is approximately 18° counterclockwise from the top. The cluster population in the large spiral NGC 5754 (*left*) stands out in color as well as brightness. In the companion galaxy NGC 5752 (*right*), the clusters are brighter and more neutral (redder) in color; reddening in the dust lanes as well as from more diffuse material on the south side of the galaxy is well shown.

for the NGC 5752 data, taken in the PC CCD with relatively low background. We follow the prescription of Dolphin (2000) in evaluating these, recognizing that the complex brightness distribution makes these corrections approximate. For the faintest clusters we measure, at the highest instrumental y-coordinates, the correction is only 0.025 mag in B, with a differential $B-I$ correction of -0.006 mag. Using the prescription from Whitmore et al. (1999a) gives slightly higher values (0.04 mag in B), but these effects are still swallowed up in the other photometric errors for these clusters.

Near the bright nucleus of NGC 5754 some nonexistent objects appeared in the original source list simply as a result of the greater Poisson noise and amplitude of local image structure. We rejected these based on a median-windowed image, which removed most of the effects of a strong brightness gradient on the object-finding routine.

At the distance of either galaxy pair, genuine SSCs should be at most marginally resolved by WFPC2. However, since some of the detections in nearby systems such as NGC 4038/9 have dimensions of a few hundred parsecs, being perhaps better described as superassociations, we did not require candidate clusters to be completely stellar in structure for inclusion. This may also include some blended sets of clusters, which can sometimes be distinguished by image structure. At these distances and our magnitude limit confusion between candidate clusters and supergiant stars will not be an issue, since $B = 26$ at the distance of NGC 6621/2 corresponds to $M_B = -8.6$. As found for the Antennae by Whitmore et al. (1999b), the contribution of the brightest stars is important only fainter than $M_V = -8$ and negligible for $M_V > -9$, so even the bluest of these will not be significant contaminants in our B data. Likewise, to these magnitudes, background galaxies are not major sources of contamination.

We deal with two subsets of cluster candidates for each pair—a large sample selected for 4 σ significance in B and one culled for color accuracy, with $\sigma(B-I) < 0.2$. Photometric errors are based on photon statistics for aperture photometry and fitting errors for PSF-fitting measures. The

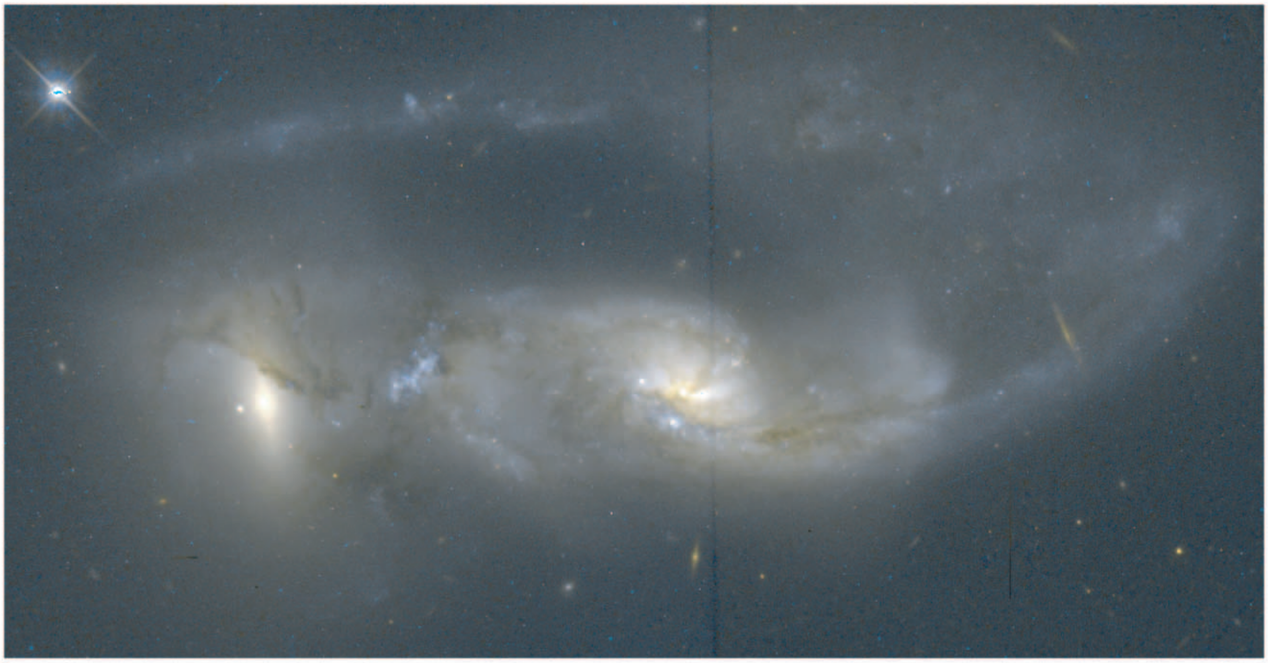

FIG. 3.—WFPC2 imagery of NGC 6621/2, again shown in a color composite incorporating a synthetic green band taken as the mean of *B* and *I*, with a pseudologarithmic intensity scale. The region shown is 64″ × 122″, and north is 46° clockwise from the top. A rich population of bright blue clusters and highly structured dust absorption are clearly shown. A small patch of dust nearly in front of the nucleus of NGC 6622 (*left*) is nearly lost in this display.

color samples have effective limits near $B = 26$, somewhat depending on local background intensity. For NGC 5752 we removed about 40 faint cluster candidates (all fainter than $B = 23.5$ and most fainter than $B = 25$) if their peak surface brightness was no higher than that found in an extended background region. This was to reduce false detections produced by clear patches between the prominent dust lanes.

2.3. *Fiber-Array Kinematic Data*

To help understand the kinematics and interaction history of NGC 6621/2, we measured the velocity field in Hα and [N II] emission using the 3.5 m WIYN telescope and Dense-Pak fiber array. As described by Barden, Sawyer, & Honeycutt (1998), the array includes a 7 × 13 configuration of fibers in a roughly hexagonal packing covering a 35″ × 45″ region, rotated for these observations to P.A. = 114°, to put the long axis approximately parallel to the galaxy separation in this pair. Four outlying fibers allow sky subtraction far from the galaxy centers. During 2000 June 19–20, four 25 minute exposures were obtained in each of two regions, roughly centered on NGC 6621 and NGC 6622. Each of these sets was dithered in a parallelogram pattern, with each leg offset by about 2″, to fill the gaps between 3″ fiber apertures. The instrumental resolution with these fibers was 1.6 Å, well sampled by the 0.68 Å pixel scale. The spectral range observed was 6000–7400 Å. Velocity maps were produced from the Hα and [N II] λ6583 measures; for each observation emission was detected in 43–57 fibers, for a total of 402 velocity measures. The velocity maps were constructed on a 1″ grid, with overlapping aperture data averaged at each pixel and numerical 0″.1 subpixels used to track aperture outlines until the final averaging. Registration to the direct images used reconstruction of continuum and Hα images from the spectral measurements, giving positions of the galaxy nuclei and the bright cluster of H II regions between the two.

The resulting velocity field is shown in Figure 4. The long-slit velocity slice from Keel (1996) is also plotted for comparison, preserving somewhat better spatial resolution across the star-forming complex between the two galaxies. The rotation curve is sufficiently asymmetric that this pair (also known as CPG 534) was used in that paper as the type example for how different ways of measuring redshifts from rotation curve can differ for disturbed galaxies. In fact, we differ in our conclusions from the study by Reshetnikov & Silchenko (1990) as to the sense of the encounter. They derive a low radial velocity for NGC 6622 and conclude that the encounter is retrograde, noting that the inner disk gas is rotating in the same sense as the outer tidal features. We have no good explanation for this velocity discrepancy. In retrospect, they may have been unlucky in selection of spectroscopic position angles for analysis; our velocity data are in reasonable agreement for regions in common. Furthermore, the velocity field may be so strongly disturbed as to make a set of tilted circular ring orbits an inappropriate model in this system.

We use the WIYN spectra to address the redshift of NGC 6622. Because there is strong line emission around it, which is associated with the distorted disk of NGC 6621 and shows continuous velocity behavior across the center of NGC 6622, it is unclear whether previously published redshift values, especially from emission lines, actually reflect the stellar component in NGC 6622. While the red region we observed for gas kinematics is not ideal for absorption-line redshifts, it includes the Na D lines at this redshift and several weaker features, such as the red Ca features near 6450 Å. Summing the four fiber spectra best centered on NGC 6622, we can measure and resolve the Na lines (giving a

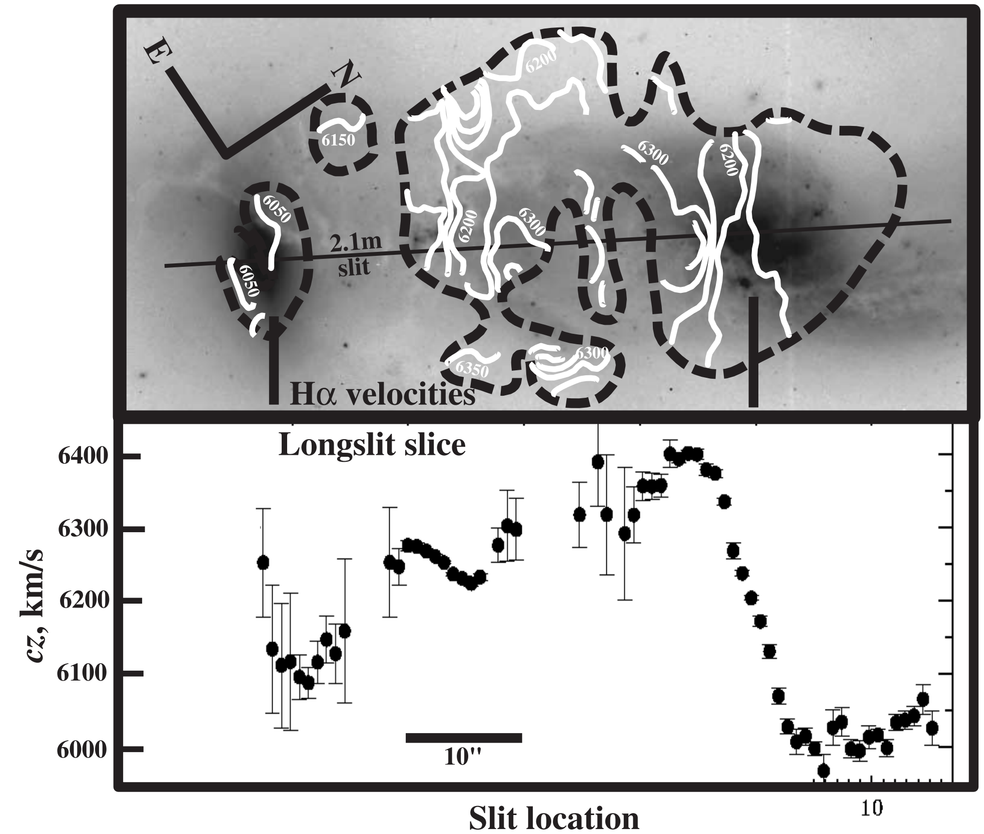

FIG. 4.—Radial-velocity data for the NGC 6621/2 system. The upper panel overlays the WIYN fiber-array velocity field on the WFPC2 *I* mosaic. The dashed curves outline the regions with detected line emission. Labelling of the contours is intended to be sufficient to show the direction of slope in each region. The sampling apertures were 3″ in diameter, setting the spatial resolution of the combined velocity map. The bottom panel shows a velocity slice across the midline of the system (along the thin line in the image) from long-slit data (Keel 1996, with $\pm 2\,\sigma$ error bars), with somewhat higher spatial resolution, showing the velocity structure across the powerful star-forming region between the two nuclei. The data sets are aligned so that corresponding points match along the *x*-axis. The nucleus of NGC 6622 has an absorption-line radial velocity $cz = 6241 \pm 10$ km s^{-1}, putting it close to the leftmost point of the long-slit data. This is important in confirming that this encounter is in a direct sense, as indicated by numerical simulations like that shown in Fig. 13.

Gaussian velocity dispersion of about $\sigma_v = 315$ km s^{-1}). The Na D equivalent widths, 1.7 and 1.6 Å, are not much larger than those predicted from stellar population models, so that interstellar absorption from foreground material does not dominate their measured wavelengths. We also see weak emission in [N II] and filling of expected Hα absorption at the nucleus, close to the stellar radial velocity. The mean redshift from the sodium lines, $cz = 6224 \pm 10$ km s^{-1} in the heliocentric frame (within 1 km s^{-1} of the observed frame for this galaxy within 2°.2 of the ecliptic pole), agrees well with the value $cz = 6241 \pm 10$ km s^{-1} that we derive by cross-correlation of the NGC 6622 spectrum, excluding the region near the Na D lines, against a spectrum of M32 obtained with the same instrument in 2000 December. This is in contrast to a substantially lower velocity of 5870 ± 100 km s^{-1} reported by Reshetnikov & Silchenko (1990). The sign of the relative velocity is important in understanding the pair's dynamics; our measurement indicates a direct encounter, which fits with the pair's overall morphology.

2.4. *Ground-based* Hα *Imaging*

To illustrate the surroundings of these pairs and provide complementary emission-line data on candidate clusters, we use ground-based *R* and Hα imagery obtained at the prime focus of the 4 m Mayall telescope at Kitt Peak National Observatory, using a 2048 × 2048 Tektronix CCD. Hα and [N II] emission was isolated using a filter nominally centered at 6709 Å shifted to about 6690 Å in the converging f/2.8 beam, with a FWHM of 71 Å. We used *R*-band images for continuum subtraction, noting the requisite flux correction factor based on the ratio of filter widths in deriving the Hα + [N II] fluxes. At 0″.42 pixel^{-1}, the field includes wide areas around each pair, which proved helpful in reducing problems from a reflection of the telescope pupil by keeping the galaxies inside the central "hole" in this reflection. Surface-brightness calibration was carried out in *R* using the NGC 7006 standard field as observed by Odewahn, Bryja, & Humphreys (1992). The narrowband image of NGC 6621/2 suffered from poor focus. The *R*-band image was convolved with a differential point-spread function (PSF) to match the narrowband image before continuum subtraction. This still leaves significant residuals near the nucleus of NGC 6622, as seen by comparison to the residuals near similarly bright stars.

Comparing the detections in Hα and in the high-resolution *HST* continuum images is important in constraining the ages of clusters, and in giving hints as to how we should interpret a similar census of H II regions in other galaxies from ground-based images. The surface-brightness sensitivity of the *R* images is also helpful in finding faint outer tidal features, as in Figure 1. Minor-axis diffuse Hα structure in NGC 5752 may indicate a starburst-driven wind.

The ionizing clusters are well enough separated in NGC 5754 that we could derive Hα equivalent widths for most of the *HST* detections, fitting PSFs derived from star images and constrained to lie at the locations measured with WFPC2. For H II regions that are not strongly decentered from the starlight this will give improved accuracy in deblending partially overlapping images. To do this, we resampled the KPNO images to match the coordinate systems of WFPC2 mosaics, with object coordinates transformed from individual CCDs to the same mosaicked pixel space. The IRAF implementation of the DAOPHOT NSTAR (Stetson 1987) routine was used to fit the fluxes of clusters in both R and Hα + [N II]. This process does not account for all the Hα emission; some is associated with clusters that are fainter than our error cutoff near $B = 26$, some may be associated with optically obscured ionizing sources, and some of the arm emission may be truly diffuse. Cluster crowding in NGC 6621/2 means that we can derive Hα equivalent widths only for larger groupings of clusters and show evidence that some of the nuclear Hα concentration arises in an outflow.

The R images, with wide-field and deep surface brightness sensitivity, are also useful in estimating luminosity ratios of the systems, particularly NGC 5752/4. Here, we assume symmetry across the overlap regions, and derive an R-band intensity ratio of 5.1 for the two galaxies, within an isophotal level corresponding to a mean radius of 90″.

3. NGC 5752/4: ONE WITH A STARBURST, ONE WITHOUT

3.1. *Dynamics and Interaction History*

The kinds of tidal structures seen in galaxy pairs can often show important facets of their dynamical history. Some of the patterns seen in n-body simulations are robust to such parameters as halo/disk ratio and disk thickness. In general, higher orbital inclinations of the companion with respect to the target galaxy's disk plane yield more asymmetric tidal structure, and direct encounters produce larger scale and more coherent tidal responses than do retrograde encounters. We use the results from the simulation survey by Howard et al. (1993) to deduce the kinds of encounter involved in these two pairs and estimate the time since strongest perturbation. Their models incorporated 150,000 "star" particles and 30,000 "gas" particles, distinguished by initial velocity dispersion, and tracked their in-plane motions (while allowing the point-mass companion to move and respond in three dimensions). Halo/disk ratios of 1 and 10 were considered, modelled as inert Mestel disk distributions; the difference generally amounts to having stronger fine structure in the low-halo case, as disk self-gravity becomes more important. This model matching will be less exact than attempts to simulate a single system in detail, but we can exclude large parts of parameter space and derive bounds on possible values of orbital inclination, mass ratio, and impact parameter.

NGC 5754 shows a rich variety of structures that can be compared with simulations, well shown in the wide-field depiction of Figure 1 and highlighted with our orbital reconstruction in Figure 5. An inner two-armed grand-design spiral pattern twists around more than 360°, with a single tidal narrow arm, not clearly extending the inner pattern, wrapping 270° around the side projected toward the companion NGC 5752. One of the inner arms has a prominent kink northeast of the core, where several luminous clusters and H II regions occur. A fan-shaped feature ("spur") extends outward from one of the arms on the northwest and northern sides of the inner disk, with a more diffuse counterpart to the south and southeast. NGC 5752 shows a long tidal tail stretching away from NGC 5754; a similar feature stretching inward would be lost against the bright disk of the larger galaxy. The WFPC2 image shows a sheet of dust in NGC 5752 tracing a well-defined plane seen nearly edge-on, along the projected major axis, which suggests that it too is a disk system.

We find the best overall fit to the structure of NGC 5754 from an encounter inclined 60° to its disk plane, with halo/disk mass ratio of 1, from a low-mass companion passing just outside the disk. The mass ratio derived this way, certainly between 0.1 and 0.5, is comparable to the R-band flux ratio of the galaxies, 0.20. Figure 5 illustrates the model structure two disk-edge rotations after the initial close passage. This model reproduces the asymmetric (if not quite one-sided) outer tidal arm, as well as the inner grand-design pattern and fan-shaped disk structures. It also gives a change in pitch angle for the northern arm at about the observed location. The uncertainly in inclination is $\pm 15°$, since there are no good fits for 30° or polar encounters. The mass ratio could be 0.1–0.4, somewhat degenerate with perigalactic distance, constrained to be from 1–2 radii of the initial disk (which itself corresponds closely to the extent of the current grand-design pattern, based on comparison of the model and image). The timescale can be set from the simulation, given kinematic information on the system, since the orbital period at the edge of the initial Mestel disk was set to 100π time steps. This radial location corresponds to 36″ (11.3 kpc) based on the structural match in Figure 5. We derive a circular velocity 285 km s^{-1} from the H I profile parameters given by Haynes & Giovanelli (1991), noting that their orientation estimate of 25° from face-on is close to the 27° that we estimate from comparison with the face-on model. These values give a rotation period at this radius of 220 Myr, and a time step of 0.70 Myr. The best-fit model is seen 350 time steps after perigalacticon (which occurs at time step 100 in the simulation shown in Fig. 5), so this pair represents a relatively weak perturbation that has developed through $\approx 2.5 \times 10^8$ yr. The fit is distinctly worse for models ± 50 time steps from this, so 50 steps or 35 Myr is a reasonable error estimate.

Tidal distortions in the morphology and radial profile of NGC 5752 add clues to its orbital history. As discussed by Johnston (1998 and references therein), tidal disruption of a small companion galaxy results in stars becoming unbound and preferentially streaming in tails oriented roughly along the orbit. Nearby examples include the Magellanic Stream and the recently identified tidal debris from the globular cluster Pal 5 (Rockosi et al. 2002). As shown in Figure 1, NGC 5752 has a long, low surface brightness tail extending outward in projection from NGC 5754; any such feature in the opposite direction would be lost against the much brighter structure in the larger galaxy's disk. An isophotal twist occurs between the inner disk of NGC 5752 and this tail, accompanied by a break in the slope of the surface brightness profile and a change in the image ellipticity. These are shown in Figure 6, from the results of using the STSDAS ELLIPSE task to fit the KPNO R-band image, excluding the regions toward NGC 5754 where spiral

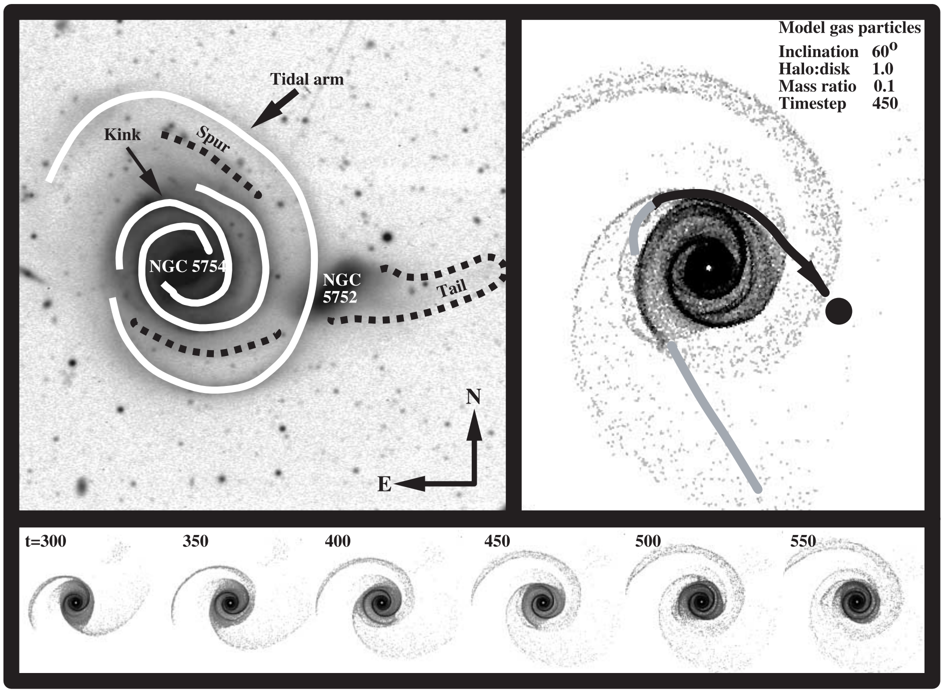

FIG. 5.—Simulation and our orbital reconstruction of the encounter of NGC 5752/4. The *R*-band image (*left*, as in Fig. 1) has been annotated to show the important tidal structures we attempt to match from the simulation. The best-matching numerical simulation is shown at the right to the same scale and orientation (found for an inclination 26° from face-on). The relative orbit of NGC 5752 is shown approximately, with the gray curve indicating portions behind the disk of NGC 5754; uncertainties in the system's inclination make this less accurate then the match of structures in NGC 5754. The sequence at the bottom shows the simulation from which the best match was drawn, at intervals of 50 time steps or 35 million yr; the enlargement on the right shows the fourth of these at $t = 450$. Perigalacticon occurs at $t = 100$ time steps, so our view is 250 Myr later. The features matched include the presence of an inner grand-design spiral, the strong asymmetry in intensity between the two outer tidal arms, and the location of the two spiral "spur" features and the northern kink in the main spiral pattern. The simulation frames represent "gas" particles, which show the characteristic structures more clearly than the "star" particles and will represent young stellar populations more closely. The asymmetric tidal arms are also present at later times, but the spiral "spurs" fade at later time steps.

structure is bright and difficult to model easily. Such a set of signatures appears in models for the disruption of companion galaxies presented by Johnston, Choi, & Guhathakurtha (2002) and Choi, Johnston, & Guhathakurtha (2002). They show that the morphology of tidal debris depends on orbital eccentricity, phase, and viewing direction, and they suggest ways to distinguish whether the dominant mechanism for loss of stars is tidal stripping (in near circular orbits) or heating (for more eccentric paths). If the break in the intensity profile occurs at the same radius as the change in shape and orientation of the fitted ellipses ($r_{\rm break} \approx r_{\rm distort}$ in their terminology), heating is dominant and the orbit has high eccentricity. For near circular orbits, or near the apses of eccentric orbits, stripping dominates, so that isophotal twisting which can be important well within the break radius ($r_{\rm break} > r_{\rm distort}$). From Figure 6 $r_{\rm break} = 25''$ in this case, while distortion begins well inward of this, $r_{\rm distort} \approx 16''$. The photometric profile is thus consistent, although not uniquely so, with our *n*-body interpretation, in which the initial path is parabolic (before energy exchange at the first encounter). The direction of the tidal debris also gives a hint at the orbital orientation, in the sense that the rotation of position angles between the galaxy's disk and tidal debris should go toward the direction of the orbit (as shown, for example, by Johnston et al. 2002). Even the inner parts of NGC 5752 might be significantly prolate from tidal effects, although the dust structure shows that disk symmetry is still dominant. While the mass ratio in this pair makes the tidal impulse seen by NGC 5754 relatively weak, NGC 5752 has undergone a much stronger perturbation, although there is a smaller radial distance over which it could operate.

3.2. *Star Clusters and* H II *Regions*

The WFPC2 data reveal a rich population of clusters in each galaxy, with very distinct properties. These offer an interesting comparison, especially in regard to the different levels of tidal perturbation encountered by the major and minor partners in the interaction, as well as clues to when and where cluster formation can be triggered. An overview of these populations is shown in Figure 7, where the spatial distribution of clusters is coded by their *B* magnitudes.

3.2.1. *A Starburst in NGC 5752*

NGC 5752 hosts numerous bright clusters, with a nearly flat differential luminosity function from $B = 21.6$–26. At the faint end, crowding is clearly an issue—the configuration is so small in projection that there is little room for faint sources to be detected. The clusters span a broad color range $B-I = 0.6$–2.2, with no particular evidence of color-magnitude relation. Our criterion for useful color measurements of $\sigma_{B-I} < 0.2$ retains 139 clusters out of 306 detected to $B = 26$, with the errors dominated by background noise from adjacent objects in the "sky" annuli. Confusion between genuine clusters and fine structure in the dust may set in, but only fainter than about $M_B = -11$, an effect whose correction would accentuate the true degree of weighting toward bright clusters that we observe.

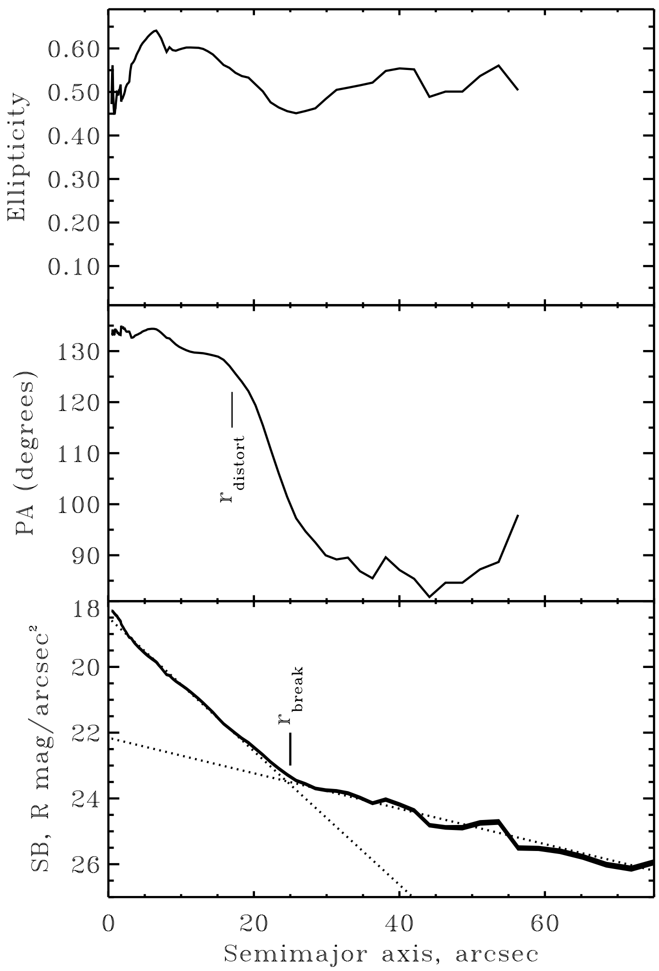

FIG. 6.—Radial profiles of the *R*-band structure from NGC 5752, derived from ellipse fitting to the western half of the galaxy to reduce contamination from NGC 5754. Following Fig. 3 of Johnston et al. 2002, we indicate distortion and profile-break radii, whose ratio suggests that the relative orbit of NGC 5752 has large eccentricity. To emphasize the break in surface-brightness profile, the two dotted lines indicate exponentials fit for $r = 2''$–$18''$ and $r > 27''$, with an outer scale length almost 4 times larger than the inner value.

A more important issue is the crowding effect of such a dense collection of star clusters, in both object detection and photometry. We removed candidates with overlapping photometric radii, retaining only the brightest of each potential set. This leads to progressively more severe undercounting of fainter clusters, as more of the available area is already taken up by brighter clusters. We estimate the effect of this crowding in two extremes. The minimum correction assumes that the faint clusters are spread uniformly across the well-populated part of NGC 5752 on the near side of the disk, about 27 arcsec^2. The maximum correction assumes that they are concentrated to the central region as strongly as the bright clusters, half of which occur within a single region of 6.0 arcsec^2. The estimated fraction of undercounting at a given flux is the ratio of total area considered to the sum of the aperture areas for all brighter clusters. For the faintest clusters with useful colors ($B \sim 24.8$), the correction is a factor 1.4 for the minimum case, up to 3.0 for the maximum case. Even the maximal correction leaves the luminosity function unusually flat in comparison to most other systems.

The color-magnitude distributions and luminosity function of these clusters are displayed in Figure 8. Both stand in contrast to the same diagrams for NGC 5754 (§ 3.2). The distribution of magnitudes is flatter, and extends brighter, in NGC 5752. The diagram includes the luminosity function after applying the "minimal" and "maximal" crowding corrections above.

An interesting paradox is that the cluster population is also redder. While NGC 5752 is visibly dusty, it is interesting that only 5% of this rich cluster population is as blue as the peak in the color distribution of the "normal" disk clusters in its neighbor NGC 5754, which would require an extensive dust distribution in addition to the obvious filaments.

The Hα emission does not appear to be associated with individual clusters, lacking peaks near bright clusters. Instead, there is strong but diffuse emission following the disk of NGC 5752, plus extended plumes along the minor axis (Fig. 9). More precisely stated, any peaks associated with the brightest clusters are too weak to stand out against the large-scale emission at $1''$ resolution. Comparison with the WFPC2 *I* image blurred to the same resolution shows that there may be a distinct peak corresponding to the two bright clusters at the left end of the central region in Figure 9, but the match to the overall cluster distribution is not close. The ridge line of Hα is offset northward from the bright central clusters, and the emission includes a significant component extending along the projected minor axis, most prominent on the south side. (Both these points are accounted for by dust absorption in the disk plane, strongly obscuring minor-axis structure on the far side.) This appearance is reminiscent of the filamentary emission from global winds in such starburst systems as M82 and NGC 3628 (Shopbell & Bland-Hawthorn 1998; Fabbiano, Heckman, & Keel 1990). Since such winds may have ionization arising from shocks, as well as from photoionization by the galaxy's overall OB star population, Hα will not necessarily give a reliable measure of the ionizing luminosity of stars in this galaxy. Virtually all the line emission is contained within a radius of $10''$, and, indeed, we see a monotonic decline in Hα + [N II] equivalent width with increasing aperture radius, from 54 Å at $5''$ to 28 Å at $12''$. These encompass the value of 43 ± 5 Å listed by Kennicutt et al. (1987). Both the star formation as traced by bright clusters and the ionized gas are more concentrated than the red starlight, strongly enough that the central Hα equivalent width within $5''$ indicates a burst of star formation unless most of the line emission is powered mechanically, rather than by photoionization. Even in that case, such energy input must reflect a transient event, so we have made a long-winded argument supporting what is clear from the presence of any luminous clusters in a low-luminosity galaxy—the interaction has triggered a burst of star formation.

Some of the clusters' color spread is certainly due to dust reddening. Several of the brightest clusters with $B-I > 2$ lie on the side of NGC 5752, where the dusty disk is in the foreground. In addition, the average color of clusters in the inner $2''$ concentration is redder than found in the surroundings, 1.9 versus 1.5. The full cluster population is certainly richer than we see at these wavelengths, with additional examples hidden behind the dusty filaments in the disk plane.

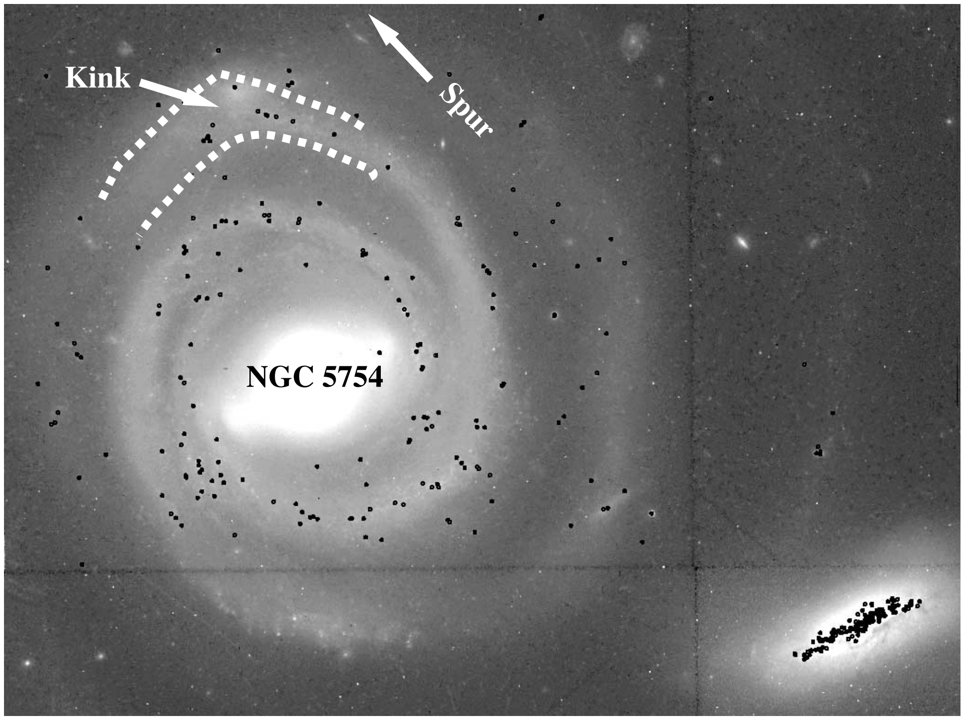

FIG. 7.—Locations of star clusters in the NGC 5752/4 system marked on the *I* WFPC2 mosaic. These comprise the "bright" sample, cluster candidates with color error $\sigma_{B-I} < 0.2$. Except in the crowded regions of NGC 5752, this corresponds approximately to $B < 26$. The orientation is as in Fig. 2, enlarged to show a region $77'' \times 104''$ in extent. The arm kink used in matching the numerical model is marked, along with the spur extending out of the frame.

3.2.2. *Normal Disk Clusters in NGC 5754*

In contrast, the clusters in NGC 5754 are fainter, and spread throughout the disk and spiral pattern. Only one of these clusters would appear among the fifty brightest (at *B*) in the smaller companion system NGC 5752. The brightest clusters in NGC 5754 are in the inner spiral pattern, just off the tips of the small bar. There are no bright clusters inside the inner ring which surrounds the bar, as is often found for H II regions in spirals with bars and rings (Crocker, Baugus, & Buta 1996). The cluster population is well concentrated to the spiral arms, a "beads-on-a-string" trend that is strongest for the brighter clusters. This is illustrated by overlaying the cluster positions on an *I* image (Fig. 7). Of the clusters bright enough to pass our $\sigma_{B-I} < 0.2$ criterion, 85% fall within the continuum spiral arms. Looking at the entire cluster sample, interarm clusters are as a group fainter than average, but faint enough that we cannot tell whether they are also redder, as would be expected if they are aging clusters which have moved outside the arm ridges where they were formed. A handful of faint, very red clusters within the ring may be genuine old globular clusters.

The color and magnitude statistics are summarized in Figure 10, which combines the color-magnitude diagram with histograms in *B* magnitude and color. All these distributions are quite distinct from the bright, redder cluster population found in the companion galaxy NGC 5752. The color span runs as blue as the bluest unreddened value $B-I = -0.3$ expected for a cluster formed instantaneously, with most clusters bluer than $B-I = 0.7$. This suggests that most of these clusters are younger than 7×10^7 yr, based on the Starburst99 models. The luminosity function in this galaxy is strongly weighted to faint clusters, again in contrast to the flatter distribution in NGC 5752, where our maximum crowding correction gives $\alpha = -1.7$.

The luminosity function of clusters can often be expressed in a simple power-law form. As noted by Larsen (2002), a power-law function in luminosity $N(L)dL = \beta L^{\alpha}$ implies linear behavior in number per unit magnitude $N(M) = b + aM$, where $\alpha = -(2.5a + 1)$. For clusters brighter than $B = 25$, a least-squares fit to the binned luminosity function (for bins with $n > 1$, using Poisson weights) has $a = 0.69$, yielding $\alpha = -2.7 \pm 0.4$. This is not unusual for a "normal" spiral disk; Larsen (2002) finds undisturbed spirals with $\alpha = -2.0$–2.5. Larsen also shows that a constant star formation rate gives a similar value $\alpha = -2.7$. However, for cluster age ranges comparable to the dynamical timescales of many interactions, the slope of the cluster luminosity function is fairly constant; Whitmore et al. (1999b) find that the bright clusters in NGC 4038/9 exhibit $\alpha = -2.6 \pm 0.2$ in *V*, with younger clusters showing some evidence of a flatter slope (as in their Fig. 18). In contrast, for the range of crowding corrections used for NGC 5752, its cluster system has $\alpha > -1.7$.

The combination of age and mass effects has made interpreting the luminosity function alone of clusters (or H II regions) ambiguous. An important role for age is suggested by the reddening of mean colors for fainter objects in NGC 5754 (as in Fig. 10). However, potential selection effects make it difficult to make such a case from the WFPC2 data alone, since extreme colors will drive up the $B-I$ error and drop clusters from the sample, and systematic behavior of reddening with location across spiral arms could mimic age behavior as well. Multiple continuum colors can improve the situation, as can emission-line information. We can further examine the history of cluster formation in NGC 5754 by comparing continuum colors with Hα equivalent widths, using a hybrid data set of *HST* aperture photometry and KPNO Hα data. The Hα fluxes and associated *R* continuum fluxes were measured by PSF fitting on the KPNO

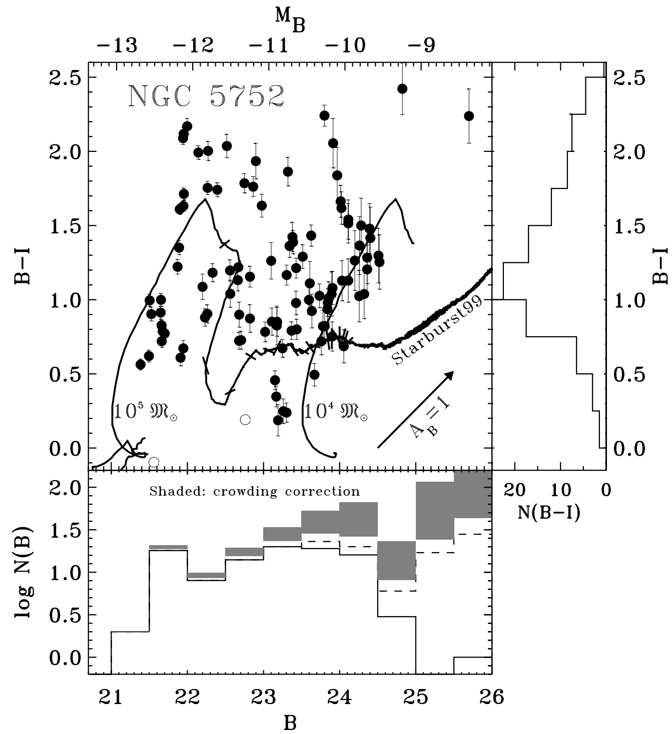

FIG. 8.—Color-magnitude diagram for clusters in NGC 5752, including those with errors $\sigma_{B-I} < 0.2$. The wide color spread is independent of magnitude, and the differential luminosity function (shown in number of clusters per 0.5 mag bin) for detected clusters is nearly flat from $B = 21.5$–24.5; the dotted histogram includes clusters which do not satisfy the color error criterion for the main panel, which are most detections at $B > 24.5$. The two uppermost histograms show this distribution after applying our minimum and maximum crowding corrections. The two brightest clusters from NGC 5754 are shown as open circles for comparison with Fig. 10. The effective magnitude limit for this sample is probably no fainter than $B = 24.5$, limited by crowding in the inner part of the galaxy. The color evolution of a single cluster (scaled to $10^5\ M_\odot$) is shown from the Starburst99 output described by Leitherer et al. (1999), as is a reddening vector for this filter system and a young stellar population. The age of the Starburst99 models is shown by cross marks every 5×10^6 yr up to 10^8; the first of these is almost lost in the initial loop near $B-I = 0$. The reddest color in the model occurs at 8.6×10^6 yr as red supergiants reach their peak contribution. Part of this red loop (from 5–10 Myr) is repeated for reference at a stellar mass of $10^4\ M_\odot$, showing that the masses of the detected clusters mostly lie in the range 10^4–$3 \times 10^5\ M_\odot$. The right-hand panel shows the color distribution of all clusters plotted in the color-magnitude array.

images at cluster locations fixed from the *HST* identifications. As shown in an overlay of the Hα image over the WFPC2 *B* data (Fig. 11), much of the line emission is associated with identified clusters. By the same token, most of the bright clusters have Hα counterparts, which immediately shows that they are bright because of youth rather than extreme mass. The line emission reflects young, massive stars, type B0 and hotter, so its strength changes dramatically with age over time spans that leave $B-I$ nearly constant. The comparison is thus sensitive to the ages of clusters and the distribution of ages in the sample. These data (Fig. 12) show an envelope of decreasing Hα EW for redder clusters, indicating that age is a more important factor in the color spread of this cluster population than is reddening. If these clusters are single-burst systems formed over less than a few million years, the youngest we see is about 8×10^6 yr old, with many at ages up to about 1.5×10^7 yr. If each cluster we see incorporates stars formed over a span of a few 10^6 yr, the derived ages are smaller, since the $B-I$ color will reflect significant contributions from the first stars to form red supergiants while the Hα equivalent width is dominated by younger, hotter members. Durations of a few million years for each star-forming event (cluster) would account for the maximum observed Hα equivalent width near 200 Å and the distribution of observed colors and equivalent width for the cluster population.

3.3. *History of Cluster Formation*

The NGC 5752/4 system provides a striking contrast between disks which underwent dramatically different levels of tidal perturbation at the same time. Nothing very unusual seems to happened in NGC 5754; its cluster population is comparable to other similarly luminous spirals such as NGC 6946 and NGC 4258 from Larsen (2002). In contrast, NGC 5752 has hosted a starburst with a rich population of very luminous clusters. This is consistent with the idea that there is a minimum level of tidal influence needed to trigger the formation of these massive clusters.

The clusters in NGC 5752 are unusually red and have a wide color range, which fits with the observed dust structure in suggesting substantial reddening. None of the clusters in NGC 5752 is as blue as the population in NGC 5754 over the same magnitude ranges. The least reddening that we can assign without multicolor data assumes the clusters to be concentrated in age so as to populate the reddest excursion in predicted colors, around 1.2×10^7 yr. Most clusters would have to fall in this range, however, and about one-third of them still require foreground dust. Combining dust and age fading, this population of clusters must have been even more spectacular a few times 10^7 yr ago.

In this instance much of the cluster formation must have been confined to this short span. The evidence for an outflow raises the possibility that cluster formation has been terminated by loss of dense gas, which might be related to the flat (or even peaked) luminosity function of these clusters. Such a distribution is particularly interesting as a possible step toward the narrow Gaussian luminosity function of globular clusters. By analogy with formation of stars in such regions as the Eagle Nebula, we might speculate that lower mass clusters would suffer first as a wind develops.

4. NGC 6621/2: RAPID RESPONSE TO A STRONG PERTURBATION

4.1. *Dynamics and Interaction History*

The major tidal feature in NGC 6621 is the extensive one-sided tidal arm wrapping to its north. Additional starlight and H II regions span the region between the galaxy nuclei, and continue past the core of NGC 6622. A dust lane in front of NGC 6622 shows a helical twist, which indicates that it is close enough in three dimensions to be strongly accelerated by the smaller galaxy's potential. As in the case of NGC 1409/10 (Keel 2001), such twists may be a signature of pairs favorable for mass transfer between members. NGC 6622 shows a narrow edge-on disklike structure spanning the inner 7″ and a dust feature spanning about 1″.5 (Fig. 3), inclined by about 30° to the apparent stellar disk and not obviously connected to the extensive dust in NGC 6621. This is the only disturbed feature of NGC 6622. The emission-line velocity field (Fig. 4), and new redshift

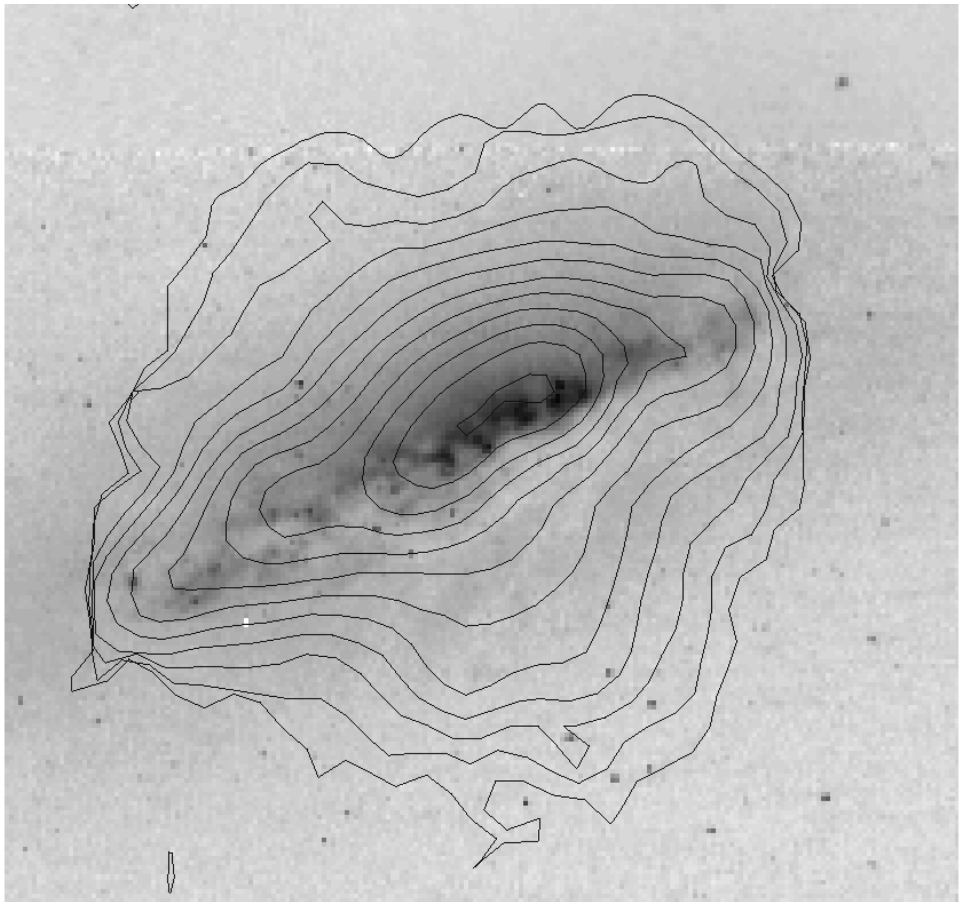

FIG. 9.—Hα + [N II] emission from NGC 5752, shown as contours overlaid on the F450W WFPC2 image. The region shown is 20″ square, with the contours spaced logarithmically at intervals of 0.2 dex and the image also logarithmically mapped. The orientation is as in Figs. 2 and 7, with north 18° counterclockwise from the top. The WFPC2 image as shown has been mosaicked, losing some resolution, because the PC frame includes no objects suitable for tying together the astrometric frames of WFPC2 and the Hα image. The minor-axis plume suggests that much of the Hα emission is associated with a global wind, while the poor match to the cluster distribution indicates that very little of the emission comes from H II regions around individual ionizing clusters.

measure for NGC 6622, confirm the directions of relative motion as being a direct encounter for NGC 6621 and nearly polar one for NGC 6622.

The extensive tidal disruption in NGC 6621/2 immediately suggests a mass ratio near unity, and a small impact parameter. Indeed, we find the best morphological match for equal-mass galaxies, closest approach near the disk edge and much less than two disk radii, unit halo/disk ratio, and an early time. We are then seeing this system within half an initial disk-edge rotation period of closest approach, corresponding to a time since perigalacticon of about 1.0×10^8 yr using the inner symmetric rotation curve in Figure 4. As shown in Figure 13, this model reproduces the extensive splash of material between the galaxies, the strongly curved tidal arm on the opposite side, and even the presence (though not the distribution) of material diverging from a close approach to NGC 6622. The behavior of such material depends strongly on the perigalacticon distance, mass distribution and precise location of NGC 6622. In this pair, NGC 6621 is undergoing a strong perturbation, and we view it shortly after closest approach and maximum tidal stress. Since our target pairs were selected from tidal morphology, it is no coincidence that the best match in each case is for a direct encounter.

Seeing NGC 6621/2 early in a strong encounter may allow us a close look at where the clusters form, since there has been little time for clusters triggered by the interaction to diffuse very far from their formation sites, either as considered within the rotating disk of NGC 6621 or in the context of the overall tidal structure.

4.2. *Cluster Population*

NGC 6621 has a very rich population of luminous star clusters. They are found near its nucleus, in the inner disk largely toward NGC 6622, in a prominent star-forming complex between the two nuclei, and in the opposing tidal arm (Fig. 14). Their color and magnitude distributions are shown in Figure 15. Clusters extend as bright as $M_B = -14.6$ and as blue as the youngest modelled populations from the Starburst99 code. The color distribution peaks near $B-I = 0.8$, bluer than we see in the clusters of NGC 5752. The circled points in this plot show clusters in the complex between the nuclei, discussed in the following section.

As in the case of NGC 5754, we can fit a power law to the luminosity function at bright levels where incompleteness is not an issue. Here we derive the logarithmic slope of the magnitude distribution as $a = 0.50 \pm 0.05$ implying a

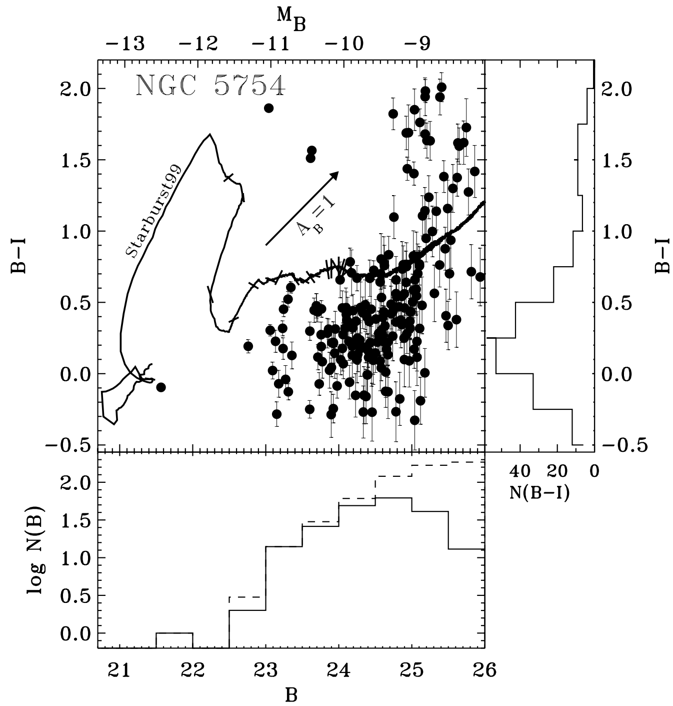

FIG. 10.—Color-magnitude diagram for clusters in NGC 5754, including those with errors $\sigma_{B-I} < 0.2$ and laid out as in Fig. 8. This population is simultaneously bluer and fainter than that seen in NGC 5752. The cluster masses must be substantially smaller as well, an effect which will be amplified by the allowed range of reddening in the smaller companion. The dashed luminosity function includes clusters with color errors larger than $\sigma_{B-I} = 0.2$, giving a sample complete to a level perhaps 0.5 mag deeper than the color sample.

power-law index in luminosity $\alpha = -2.25 \pm 0.12$, again in the range found for both normal and starburst galaxies.

There is an asymmetry in number of clusters between "inner" and "outer" halves of NGC 6621, seen in both the *HST* continuum results and the Hα structure (Fig. 16). This fits generally with tidal triggering of cluster formation, since the tidal stress has been much stronger in the region between nuclei, where we see more clusters. As a result, perturbations of the velocity field have been stronger (as shown in Fig. 4), which must logically precede disturbances in gas density or cloud separation.

Clusters, with and without strong Hα emission, are seen in the prominent tidal arms or tail to the northeast. Cloud collapse is still going on in this region, as has been noted in NGC 4676 by de Grijs et al. (2003). Indeed, the existence of H II regions in the tidal tails of NGC 4676 and 4038/9 has long shown that star formation can continue for several times 10^8 yr in gas launched well away from interacting systems into tidal features. This was reflected in the relatively strong Hα emission measured in the tails of the Mice by Stockton (1974) and in the Antennae by Schweizer (1978) and Mirabel et al. (1992). At its extreme, such processes may be symptoms of the existence of massive and self-bound clumps in the tails, such as would form tidal dwarf galaxies (although the dynamics of their formation may require a role for dark matter, as discussed by Hibbard et al. 2001).

The broad color distribution indicates that many of the clusters in NGC 6621 are significantly reddened and dimmed. From the reddest excursion of the colors in the Starburst99 models, clusters are present with at least $A_{B-I} = 0.7$, and as large as 2.0 if other models with a less pronounced redward loop are accurate. This makes the cluster population intrinsically even more impressive, especially since the second brightest cluster at B must be reddened by at least $E_{B-I} = 0.9$ which means that its corrected absolute magnitude at least as bright as $M_B = -16.3$. Several additional clusters would likewise stand only about 0.5 mag fainter with this minimum reddening correction. Cluster masses must range up to at least $6 \times 10^5\ M_\odot$ using the Starburst99 tracks. The bluest clusters give a minimum age, requiring that they be less that 10^7 yr old.

4.3. *A Massive Disk Star-forming Region*

One of the most striking features of NGC 6621/2 is the very luminous star-forming region found along the line between the nuclei, at a projected distance of 26″ or 11 kpc from the center of NGC 6621. A long-slit spectrum (Keel 1996) shows interesting kinematics in this region, with the slope of the rotation curve reversing in sign for about 2 kpc. The WFPC2 images break this region up into over 40 individual clusters, which are among the bluest to be found in the whole system. They are marked as circled data points in Figure 15. Most of the disk Hα emission comes from this area as well, also marking this as a current site of extraordinary star formation. The projected dimensions of this region are $2''.6 \times 5''.5$ or 1.1 kpc $\times$ 2.3 kpc, with the direction of elongation indicating that it is likely to be as narrow as it looks but quite possible longer; simply projection in the plane at an inclination of 70° would make it 1.1 kpc $\times$ 6 kpc, so that seen face-on this might appear a very bright piece of the spiral structure.

The overall Hα equivalent width in this region is the highest found in the entire system, at 285 Å averaged on 2″ scales. This corresponds to ages 6–7 $\times 10^6$ yr in the Starburst99 models. Star formation in this area is a recent phenomenon in comparison to the interaction timescale. Significant older populations would decrease the Hα equivalent with, and the observed distribution in $B-I$ does not allow any of the detected clusters to be older than 10^8 yr, even neglecting reddening. Obvious dust clouds near the "intergalactic" complex suggest that extinction may be important in some of these cluster colors, though it would have to exceed $A_B = 1$ to hide luminous clusters from detection. Thus, some of the cluster colors are likely to be even bluer than we measure.

5. ANALYSIS

5.1. *Formation Mechanisms for Massive Clusters*

Multiple mechanisms have been suggested as drivers for the enhanced star formation during galaxy encounters. The locations of star formation, especially in massive clusters, during the encounters we have observed may help refine the list, since some kinds of dynamical processes will operate preferentially in certain parts of the galaxies or time spans. Our own results can be supplemented with those for other well-observed and reasonably well-modelled interacting systems. The best-known is NGC 4038/9, one of the pairs whose striking tidal features inspired the original Toomre & Toomre (1972) investigation using restricted three-body calculations. Their rough orbital history has been substantially refined by successive *n*-body models of increasing

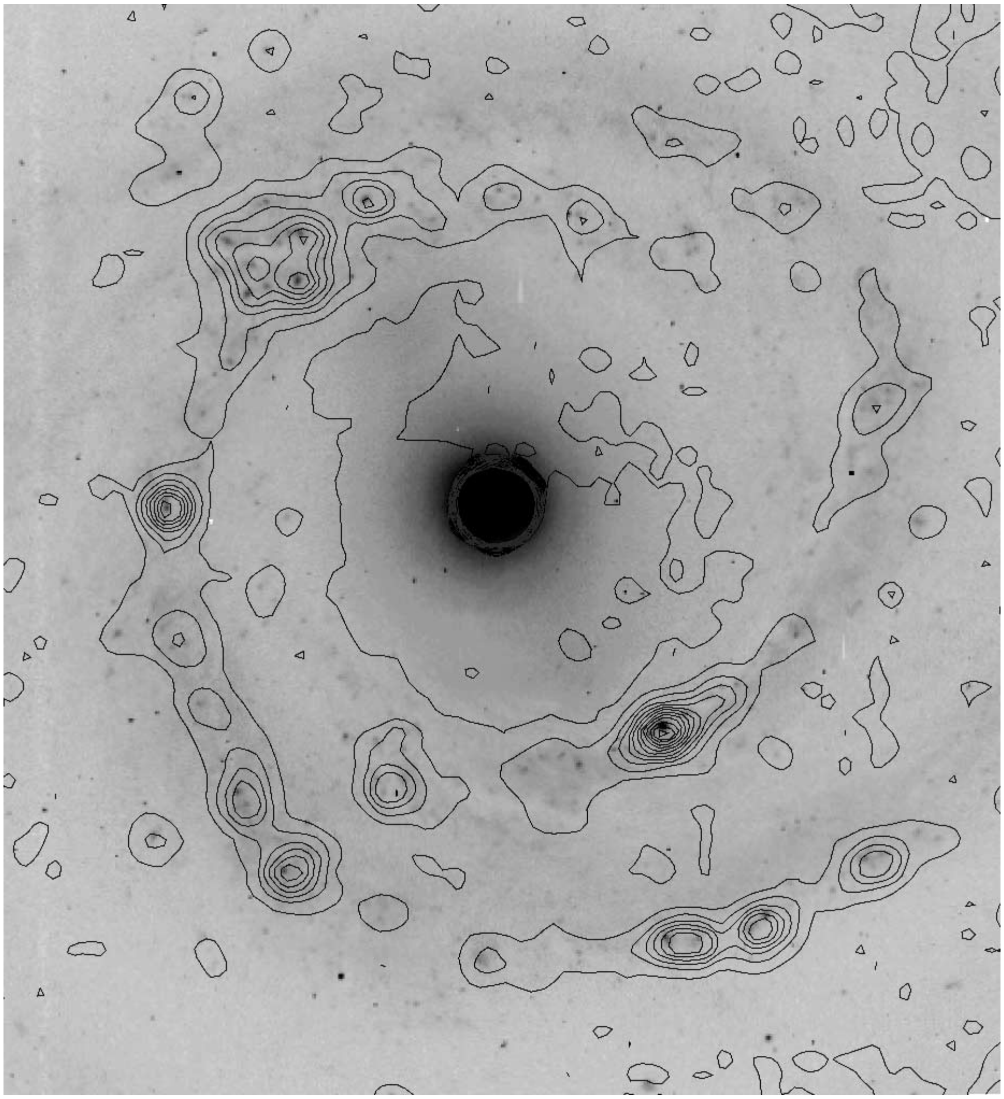

FIG. 11.—Hα contours from the continuum-subtracted KPNO image, overlaid on the WFPC2 *B* image of NGC 5754. The *B* image is displayed logarithmically, while the contours in this case are spaced linearly. This region is 50″ across. The comparison illustrates the level of correspondence between *HST* cluster detections and H II regions, which is good but not completely one to one. A good example comes from the clump of clusters to the upper right of the nucleus, where some have strong Hα and others show no influence on the Hα structure.

sophistication and accordingly better matches to the observed velocity field as well as morphology. We adopt the orbital parameters used by Barnes (1988) and Mihos, Bothun, & Richstone (1993). This puts our present view about 2.1×10^8 yr after the initial close passage between the galaxies, whose equal-mass disks had radii about 10 kpc and with a smallest nuclear separation of 13 kpc. They are now well into the second approach of a rapidly decaying mutual orbit, with the next merging passage to come in about 10^8 yr. Both disks see a passage inclined by about 60°. Since this situation is more complex than the single dominant close passage we deal with in the other systems, and the systems remain nearly in disk contact, we take this system as representing the results of an interaction seen in mid encounter.

For NGC 2207/IC 2163, we use the model described by Elmegreen et al. (2000) with refinements provided by C. Struck. These galaxies have approached on a highly eccentric relative path, with their disks grazing about 4×10^7 yr before our current view. The relative path is inclined by 25° to the disk of NGC 2207, which is the more massive galaxy by a factor close to 3. The properties of the four systems we compare are given in Table 1, including statistics of their brightest star clusters.

Collisions between molecular clouds are an obvious mechanism for driving up the star formation rate during galaxy encounters, and offer an attractive way to compress the large amounts of gas needed to make SSCs. We can rule out a necessary role for collisions between clouds from different disks by the fact that we see a rich population of SSCs in NGC 6621 whose companion is apparently an S0 system and of small radius by comparison, and in NGC 5752, which has remained well beyond the gas-rich regions of NGC 5754 during the encounter. In fact, each of these galaxies has more of the brightest clusters ($M_B < -12$) than NGC 4038/9.

Cloud collisions for clouds originating in the *same* disk should be tracked for an in-plane encounter by the locations of orbit crossing for the clouds. However, the loci of clusters in NGC 6621/2 do not match the expected sites of orbit crossings. For example, the simulation by Klarić & Byrd

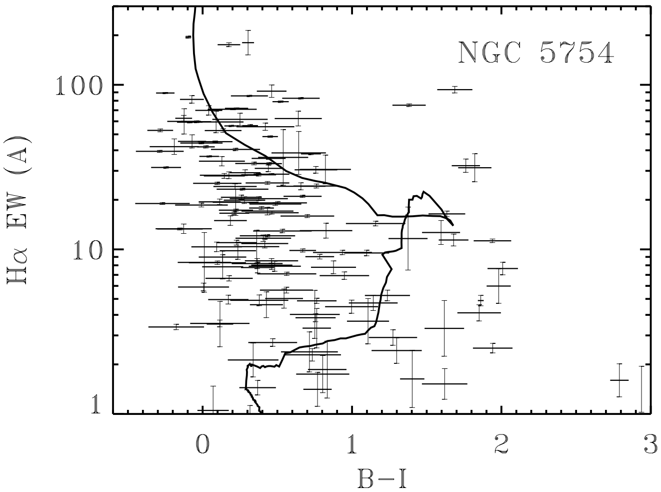

FIG. 12.—Color-emission strength relation for clusters in NGC 5754, with Hα derived by PSF fitting on the KPNO images with positions fixed to match the cluster locations from WFPC2 data. For a foreground screen, a reddening vector is horizontal, while for mixed stellar and dust distributions, the situation becomes complex. The plotted curve is the trajectory for an instantaneous burst of star formation from the Starburst99 code, at times from 5–15 $\times$ 10^6 yr (*top to bottom*).

(1990) shows the orbital streamlines for a similar encounter, in which crossing occurs predominantly on the leading edge of the bridge structure between the nuclei. The Howard et al. (1993) results give a similar picture, though in less detail because velocity information was not saved and can be only partially derived from cloud locations in successive snapshots. The star formation, as seen from both the cluster locations and Hα mapping, is concentrated near the center of the bridge region, between the nuclei, and in the opposite tidal arm. Similarly, the few luminous clusters in IC 2163 are not found in the tidal arm, shown by the Elmegreen et al. (2000) model to have rapid crossing of disk orbits from material initially in different parts of the disk. (We note that some pairs do show extensive star formation in roughly the regions expected for orbit crossing; a good example is NGC 6745.)

Another dynamical mechanism may be at work here, suggested by the flattening (and indeed local reversal) of the rotation curve near the luminous star-forming complex. Toomre (1964) presented a stability criterion for the velocity dispersion of gas in rotationally supported disks,

$$\sigma_v > 3.36 G\mu/\kappa \,, \tag{1}$$

where G is the gravitational constant, μ is the disk surface density at the relevant point, and κ is the epicyclic frequency for perturbations about a circular orbit, which may be expressed in terms of the angular velocity $\Omega(R)$ as

$$\kappa = \left(R\frac{d\Omega^2}{dR} + 4\Omega^2 \right)^{1/2} \tag{2}$$

(e.g., Binney & Tremaine 1987). This criterion is violated within radii interestingly close to the outermost star formation in many disks (Kennicutt 1989), which has been interpreted as meaning that this instability influences the overall dynamics of the interstellar medium. In a strong interaction, as seen in NGC 6621/2, the local velocity structure can be dramatically changed, and a large enough ripple in rotation velocity (and associated effective potential) can drop the epicyclic frequency κ over regions large enough to allow

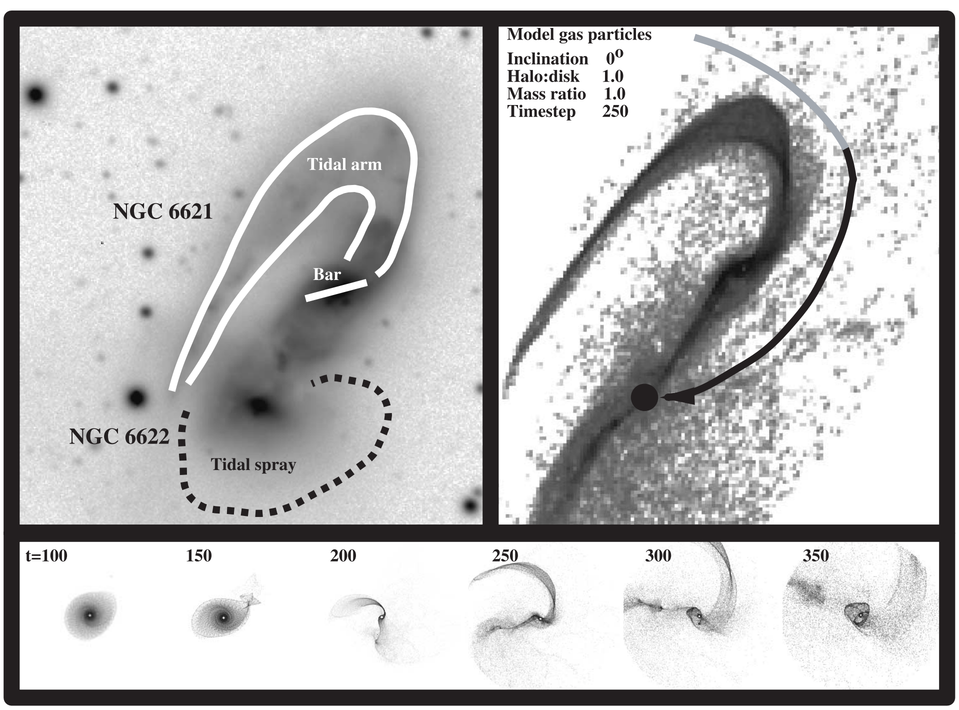

FIG. 13.—Comparison of tidal structures in NGC 6621/2 with a numerical model, laid out as in Fig. 5. The relative orbit is strongly foreshortened in this case, with closest approach occurring almost in front of the center of NGC 6621. A perigalacticon slightly farther out rapidly suppresses the extent of the tidal "spray" of particles which pass close to the core of NGC 6622, leading us to assign a closest approach somewhat greater than the precomputed model shown here. Closest passage occurs at about $t = 175$, which puts the observed configuration about 75 time steps or 1.0×10^8 yr later.

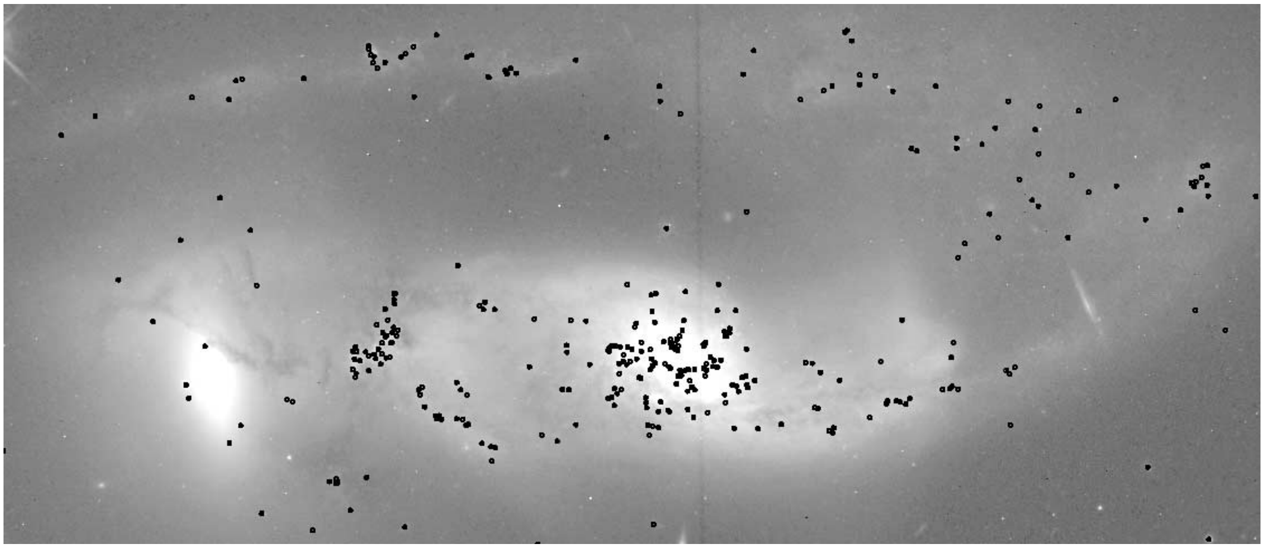

FIG. 14.—Locations of cluster candidates with color error $\sigma_{B-I} < 0.2$ in the NGC 6621/2 system, oriented as in Fig. 3. In most parts of the system, this error bound corresponds roughly to $B < 26$. This region is $40'' \times 112''$ in extent.

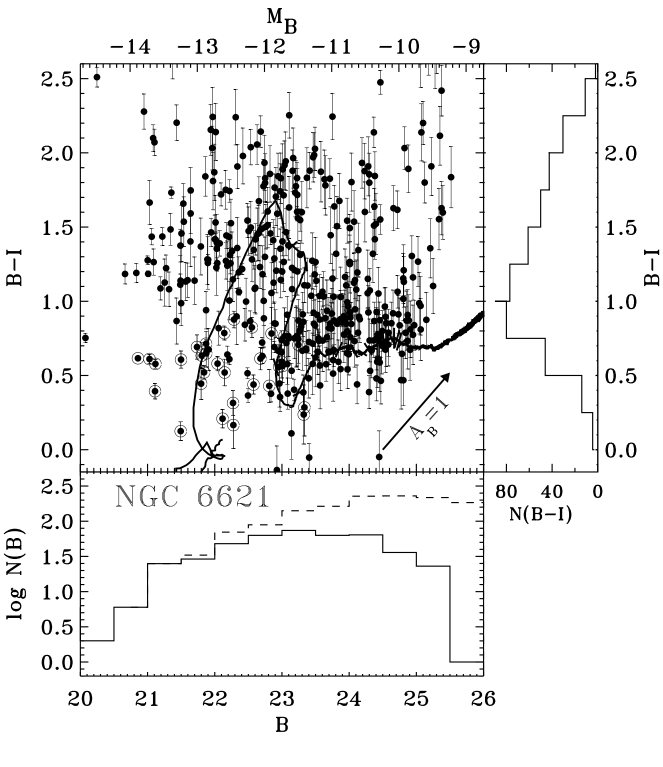

FIG. 15.—Color-magnitude array for clusters in NGC 6621/2, arranged as in Figs. 8 and 10. The peak in color near $B{-}I = 0.75$ gives limited scope for reddening of the bright clusters and requires that they be younger than about 10^8 yr from continuum colors alone. However, the blue edge to the cluster distribution suggests that the overall rate of cluster formation is now declining, and some clusters must be reddened by effective amounts as large as $A_B = 2$. Circled points indicate clusters in the crowded star-forming complex between the nuclei, which are systematically both the brightest and bluest in the entire system. The cluster luminosity function shows evidence of flattening to faint magnitudes at a level not seen in NGC 5754, despite similar overall crowding. The Starburst99 model track is the same as in Figs. 8 and 10.

substantial gas masses to go unstable. Numerical simulations (e.g., Klarić 1993) show that this instability is strong enough to allow a wide range of linear scales to become unstable on comparable timescales. This may also help explain the very large gas concentrations found by McCain (1997) in spiral/elliptical pairs, in which enough gaseous mass accumulates to alter the local disk kinematics (see also Bransford et al. 1999). The result may appear in NGC 6621 as a complex like the "interface" cloud in NGC 4038/9, but with less extinction. This is the most active star-forming site in the system, and the uniformly blue cluster colors suggest that it may have begun only recently.

It is noteworthy that the SSC populations in NGC 6621 and NGC 2207 concentrate on one side of the disks, the one toward the companion. The question of whether star-forming regions in interacting galaxies favor the (current) direction of the companion goes back at least to a debate between Arp (1973) and Hodge (1975) on the brightest H II complexes in disturbed galaxies. Arp's sample suggested that they occur preferentially between the two nuclei, while Hodge's analysis indicated that they fell opposite the companion nucleus as often as between the two. More detailed study has been hampered by projection effects; we do not always know which side of each galaxy as we see it is closer to the other one in space. Even crude matches to numerical simulations can be useful in telling which pairs we can understand well enough to recognize inner and outer sides in. If indeed SSCs are seen preferentially between the galaxies, this says that the formation trigger operates quickly and gravitationally, since it must track the current location of the other galaxy. For penetrating encounters such as NGC 4038/9, cloud collisions can act in this way, but for more distant encounters as in NGC 6621/2 and NGC 2207/IC 2163, a less direct process must be at work.

5.2. *Timing and Duration of Cluster Formation*

Most well-studied SSC populations are in currently merging systems and aging merger remnants. Our data bear on the processes happening before mergers, and in more distant encounters which happen well before the final merging

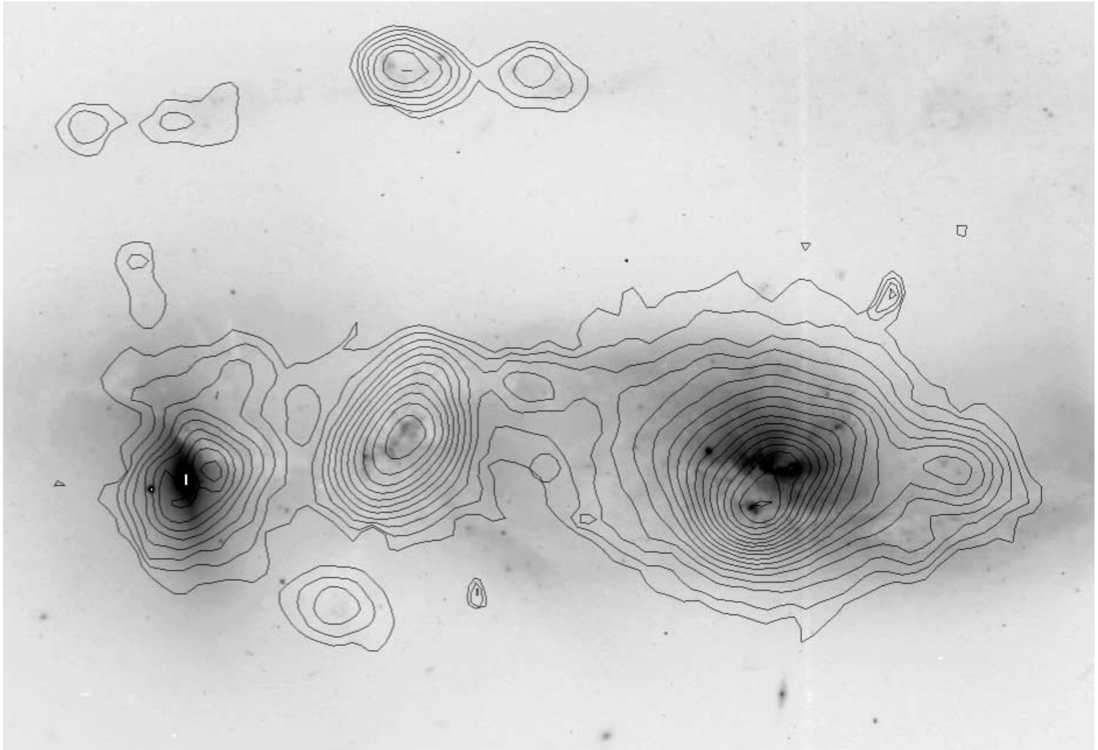

FIG. 16.—Hα contours overlaid on the WFPC2 I image of NGC 6621/2. The contours are logarithmic in emission-line intensity, at flux intervals of $\sqrt{2}$. The central peak is significantly offset from the nucleus of NGC 6621, along the minor axis, suggesting that much of this Hα emission comes from an outflow associated with the nuclear star formation. The greatest Hα equivalent width, by nearly a factor 2, is found in the star-forming complex between the two nuclei.

approach. The color behavior of SSCs in the older, post-merger systems shows a general match with the dynamical ages of these objects, so that the cluster formation is roughly coeval with merging. Looking at galaxies in earlier stages can tell more precisely when, and over what interval, cluster formation is triggered.

The bluest cluster colors in each of these galaxies show that cluster formation is continuing, extending so blue as to require cluster formation within the last 10^7 yr. This is less than the time since strongest tidal perturbation for each interaction (although the components of NGC 4038/9 are so close that it is fair to characterize this interaction as "ongoing"). Cluster formation continues for a long time after the perturbation begins and peaks, and may be delayed.

Barton, Geller, & Kenyon (2000) have found that the integrated rate of star formation in galaxy pairs, as traced from Hα emission, correlates with projected linear separation and velocity difference so as to suggest that there is a delay of a few times 10^7 yr between perigalactic passage and the onset of enhanced star formation, which lasts $\sim 10^8$ yr. Such a delay makes sense for any sort of kinematic trigger, since the velocity perturbation which responds immediately to changes in the potential much precede morphological disturbance, including changes in the distribution both stars and gas. This is consistent with the patterns we see in luminous clusters, a tracer which is detectable longer than the Hα emission. In some regions, such as the young group of clusters and H II regions in NGC 6621/2, the star formation must have set in very recently, as the cluster color distribution and overall Hα equivalent width do not allow a long history of star formation. The association of H II regions with so many luminous clusters shows that active star formation continues well after the closest approach.

The redder cluster population in NGC 5752 and the evidence for a global wind seen in Hα emission raise the

TABLE 1
INTERACTION AND CLUSTER PROPERTIES

Parameter	NGC 5754	NGC 5752	NGC 6621	NGC 2207	NGC 4038
Orbital inclination (deg)	60	60:	0	25	60
Closest passage (disk radii)	1.5	2:	1.2	1.0	0.8
Time since then (Myr)	250	250	100	40	0
Mass ratio	0.2	5	1	0.3	1
Brightest cluster (M_B)	−12.8	−13	−14.5	−14.1	−14
Bluest SSC, $B-I$	−0.1	−0.1	0.05	−0.3	−0.12
Clusters with $M_B < -12$	1	20	200	2	18

question of whether its starburst has been recently quenched as the wind removes gas from the inner regions. We certainly expect this to happen in mergers, and extension to single disturbed galaxies could be relevant to stellar population in I0 galaxies and the E+A or K+A galaxies seen in a variety of environments.

6. SUMMARY

We have studied the star-cluster populations of galaxies in the interacting pairs NGC 5752/4 and NGC 6621/2 using WFPC2 images and dynamical models. These pairs were selected to include a range of interaction age and strength of tidal perturbation, so as to help isolate the parameters that are most important in triggering the formation of massive super–star clusters. NGC 5752/4 is seen about 2.5×10^8 yr after closest approach in a system with a mass ratio near 0.2, while NGC 6621/2 is a system about 10^8 yr after a near-grazing encounter of roughly equal-mass galaxies. Their star formation responses are correspondingly varied. NGC 5754 saw a mild, if prolonged, perturbation and has a normal population of disk clusters. Its companion, which saw a proportionally stronger tidal impulse, has a rich and red population of SSCs, concentrated to the center and with a flat luminosity function. Cluster formation may have been interrupted by a starburst wind seen in Hα. NGC 6621 has a very rich population of SSCs, with young clusters concentrated in a small region between the galaxy nuclei.

This would fit with the frequent location of the brightest star-forming in pairs between the two nuclei, suggesting a nearly instantaneous trigger, and favor star formation in different locations than a cloud-collision trigger.

We have compared the SSC populations in these pairs with those of two additional pairs undergoing current interactions and for which dynamical modelling gives a fairly accurate timescale, NGC 2207/IC 2163 and the Antennae, NGC 4038/9. This comparison demonstrates several points that are important in understanding the formation of massive star clusters. Rich cluster populations do not require direct contact between the stellar disks of the galaxies, and seem to require some minimum level of tidal disturbance regardless of the time allowed for its impact to develop within a disk. Furthermore, the cluster distributions do not match predictions for the locations of orbit crossing within a single perturbed disk. The major collection of SSCs and H II regions in NGC 6621 lies in an area where the slope of the velocity field reverses, leading us to explore the idea that gravitational disturbance of a disk may allow gas to become instable by the Toomre criterion over previous stable regions, a process which could act quickly mediated solely by the perturber's gravitational influence. This would fit with the frequent location of the brightest star-forming in pairs between the two nuclei, suggesting a nearly instantaneous trigger, and favor star formation in different locations than a cloud-collision trigger.

In some regions extensive star formation has begun only recently compared with the interaction timescale, consistent with evidence for a delayed onset of enhanced star formation in interacting galaxies found from global measures. In one case, the cluster colors and Hα morphology suggest that a starburst wind has quenched the formation of new clusters. This object, NGC 5752, also shows a flatter cluster luminosity function, which might be related to the difference between power-law forms seen for young clusters in most galaxies and the near-Gaussian form for old globular clusters.

The *HST* archive is now rich in imagery suitable for surveying the brightest clusters in interacting pairs, and prospects are promising for improved understanding through additional studies involving dynamical modelling and supporting ground-based Hα data.

This work was supported by NASA through STScI grants GO-07467.01-96A,B. Thanks to Di Harmer and Gillian Rosenstein for helping make efficient use of a 4 hour break in the clouds while working at the WIYN telescope. Martha Holmes helped with the imaging at Kitt Peak, as part of an NSF Research Experiences for Undergraduates program. We thank Brad Whitmore for providing data on NGC 4-038/9 in advance of publication, and Gene Byrd for conversations on the art of reconstructing interactions. We acknowledge the public service provided by Claus Leitherer and coworkers in providing the Starburst99 code and its results for general use. Likewise, we acknowledge the value of the *z*-machine data archive recently made available by the Center for Astrophysics. Curt Struck provided his most recent model parameters for the NGC 2207/IC 2163 in advance of publication. Eija Laurikainen first mentioned the potential role of the Toomre instability to us several years ago. We thank the referee for useful comments, particularly in evaluating the role of crowding in NGC 5752.

REFERENCES

Arp, H. C. 1973, ApJ, 183, 411
Barden, S. C., Sawyer, D. G., & Honeycutt, R. K. 1998, Proc. SPIE, 3355, 892
Barnes, J. E. 1988, ApJ, 331, 699
Barton, E. M., Geller, M. J., & Kenyon, S. J. 2000, ApJ, 530, 660
Binney, J., & Tremaine, S. 1987, Galactic Dynamics (Princeton: Princeton Univ. Press), 121
Bransford, M. A., Appleton, P. N., McCain, C. F., & Freeman, K. C. 1999, ApJ, 525, 153
Choi, P. I., Johnston, K. V., & Guhathakurtha, P. 2002, AJ, 124, 310
Crocker, D. A., Baugus, P. D., & Buta, R. 1996, ApJS, 105, 353
de Grijs, R., Lee, J. T., Clemencia Mora Herrera, M., Fritze-von Alvensleben, U., & Anders, P. 2003, NewA, 8, 155
Dolphin, A. 2000, PASP, 112, 1383
Elmegreen, B. G., et al. 2000, AJ, 120, 630
Fabbiano, G., Heckman, T. M., & Keel, W. C. 1990, ApJ, 355, 442
Hibbard, J. E., van der Hulst, J. M., Barnes, J. E., & Rich, R. M. 2001, AJ, 122, 2969
Hodge, P. W. 1975, ApJ, 201, 556
Holtzman, J. A., Burrows, C. J., Casertano, S., Hester, J. J., Trauger, J. M., Watson, A. M., & Worthey, G. 1995, PASP, 107, 1065
Haynes, M. P., & Giovanelli, R. 1991, ApJS, 77, 331
Howard, S., Keel, W. C., Byrd, G., & Burkey, J. 1993, ApJ, 417, 502
Johnston, K. V. 1998, ApJ, 495, 297
Johnston, K. V., Choi, P. K., & Guhathakurtha, P. 2002, AJ, 124, 127
Keel, W. C. 1993, AJ, 106, 1771
———. 1996, ApJS, 106, 27
———. 2001, BAAS, No. 32, 1450
Keel, W. C., Kennicutt, R. C., Jr., van der Hulst, J. M., & Hummel, E. 1985, AJ, 90, 708
Kennicutt, R. C., Jr. 1989, ApJ, 344, 685
Kennicutt, R. C., Jr., Roettiger, K. A., Keel, W. C., van der Hulst, J. M., & Hummel, E. 1987, AJ, 93, 1011
Klarić, M. 1993, Ph.D. thesis, Univ. Alabama
Klarić, M., & Byrd, G. G. 1990, AJ, 99, 1461
Larsen, S. S. 2002, AJ, 124, 1393
Leitherer, C., et al. 1999, ApJS, 123, 3
Lutz, D. 1991, A&A, 245, 31
McCain, C. F. 1997, Ph.D. thesis, Australian Natl. Univ.
Mihos, J. C., Bothun, G. D., & Richstone, D. O. 1993, ApJ, 418, 82
Mirabel, F., Dottori, H., & Lutz, D. 1992, A&A, 256, L19
Odewahn, S. C., Bryja, C., & Humphreys, R. M. 1992, PASP, 104, 553

Reshetnikov, V. P., & Silchenko, O. K. 1990, Astrofiz., 33, 157
Rockosi, C. M., et al. 2002, AJ, 124, 349
Schlegel, D. J., Finkbeiner, D. P., & Davis, M. 1998, ApJ, 500, 525
Schweizer, F. 1978, in IAU Symp. 77, The Structure and Properties of Nearby Galaxies, ed. E. M. Berkhuijsen & R. Wielebinski (Dordrecht: Reidel), 279
Shopbell, P. L., & Bland-Hawthorn, J. 1998, ApJ, 493, 129
Stetson, P. B. 1987, PASP, 99, 191
Stockton, A. 1974, ApJ, 187, 219
Toomre, A. 1964, ApJ, 139, 1217
Toomre, A. 1977, in The Evolution of Galaxies and Stellar Populations, ed. B. M. Tinsley & R. B. Larson (New Haven: Yale Univ. Obs.), 401
Toomre, A., & Toomre, J. 1972, ApJ, 178, 623
Whitmore, B. C. 2000, in A Decade of *HST* Science, ed. M. Livio, K. Noll, & M. Stiavelli (Baltimore: STScI), 153
Whitmore, B. C., Schweizer, F., Leitherer, C., Borne, K., & Robert, C. 1993, AJ, 106, 1354
Whitmore, D., Heyer, I., & Casertano, S. 1999a, PASP, 111, 1559
Whitmore, D., Zhang, Q., Leitherer, C., Fall, S. M., Schweizer, F., & Miller, B. W. 1999b, AJ, 118, 1551